A Cost Optimization of Solar-Powered, Drip Irrigation Systems

by

David Doan

Submitted to the Department of Mechanical Engineering
in partial fulfillment of the requirements for the degree of

Bachelor of Science in Mechanical Engineering

at the

MASSACHUSETTS INSTITUTE OF TECHNOLOGY

June 2017

Signature of Author .....
Department of Mechanical Engineering
May 19, 2017

Certified by .....
Amos Winter
Associate Professor of Mechanical Engineering
Thesis Supervisor

Accepted by .....
Rohit Karnik
Associate Professor of Mechanical Engineering
Undergraduate Officer

A Cost Optimization of Solar-Powered, Drip Irrigation Systems

by

David Doan

Submitted to the Department of Mechanical Engineering
on May 19, 2017, in partial fulfillment of the
requirements for the degree of
Bachelor of Science in Mechanical Engineering

Abstract

This thesis presents a design and cost optimization for solar-powered, drip irrigation systems. Historical irradiance data and crop consumption data are considered and modelled during these design steps. A cost optimization is utilized in order to determine low-cost, optimum configuration that meets the required water consumption rate of a given crop. In this case, Jalgaon, India is used as an example to determine the configuration and cost per acre for solar-powered, drip irrigation systems for sunflowers, tomatoes, and barley. These configurations consisted of five 310 Watt solar panels coupled with a $5m^3$ water buffer, three 295 Watt solar panels coupled with a $5m^3$ water buffer, and three 320 Watt solar panels coupled with a $4m^3$ water buffer, respectively. These systems are projected to cost $4,600, $3,870, and $3,750, respectively. The results of this study show the value of a system optimization of solar-powered, drip irrigation systems.

Thesis Supervisor: Amos Winter
Title: Associate Professor of Mechanical Engineering

Acknowledgments

The author would like to thank Professor Amos Winter and Pulkit Shamshery of the Global Engineering and Research (GEAR) Lab for their mentorship, patience, and friendship throughout the duration of the project. I am thankful for the opportunity to work with Professor Winter and Pulkit Shamshery as they have been immensely influential in my development as a mechanical engineer and researcher.

I would also like to thank my mother, Vang Tran, and father, Chau Doan, who work endlessly to push me through school and support me in any way possible. I am also thankful for my brother, Thuan Doan, who inspires me to push myself as a mechanical engineering everyday.

To my 2.002/Thesis group, which consists of Kevin Palisoc, Stacy Mo, and Cyndia Cao, thank you for the support and encouragement through the good and bad times.

Contents

List of Figures

List of Tables

Chapter 1

Introduction

As the human population increases, resources, specifically food and water, will be heavily stressed. As water, food, and energy are inextricably linked, the cost improvement of water and energy saving irrigation systems is key to reducing this issue. This research presents a cost optimization of off-the-grid, solar-powered, drip irrigation systems in order to increase adoption of more water-efficient irrigation methods in developing countries. This model takes into account historical irradiance data, water consumption data, and hardware cost data in order to suggest a better configuration of solar panels, water pump, and water buffer that minimizes cost. In addition, this tool allows for viability assessment of solar-powered, drip irrigation systems in a given location.

1.1 Water Consumption and Scarcity

The world population is expected to increase from approximately 7 billion (currently) to between 8.8 to 10 billion by 2050, an astounding $25-43\%$ within the next 30 years [4]. With this population increase, a greater increase in food and water consumption is inevitable. Food consumption, and therefore water consumption, is expected to roughly double by 2050 [5]. This demand was observed between the 20th and 21st century when the world population nearly tripled, and consequentially the water consumption increased by six fold [6]. It is estimated that irrigation accounts for

over 85% of worldwide water consumption and on average, water consumption for food growth is 70 times higher than that of domestic usage [6, 7]. Because water consumption is heavily dictated by food consumption, water scarcity in this paper will refer to the lack of water available for agricultural usage.

1.1.1 Water Stress and Scarcity Indicators

The Falkenmark Water Stress Indicator, or commonly referenced as the Falkenmark Indicator, is the most commonly referenced method of measuring water availability per capita (Figure 1-1). Taking into account domestic, agricultural, and industrial usage, $1,700m^3$ of water availability per capita per year is the threshold for determining water scarcity [6]. Another indicator, the Water Resources Vulnerability Index, which measures water scarcity as the ratio of the total annual water withdrawals to the total water available, is also a commonly referenced method. This index uses 40% as the threshold for determining water scarcity [6]. Both of these methods show, for current and future years, water stress and scarcity in the regions of northern Africa, the Middle East, and West to Central Asia [1, 8]. In order to reduce water consumption and increase water security in these areas, more efficient, or more 'crop per drop,' irrigation methods must be explored.

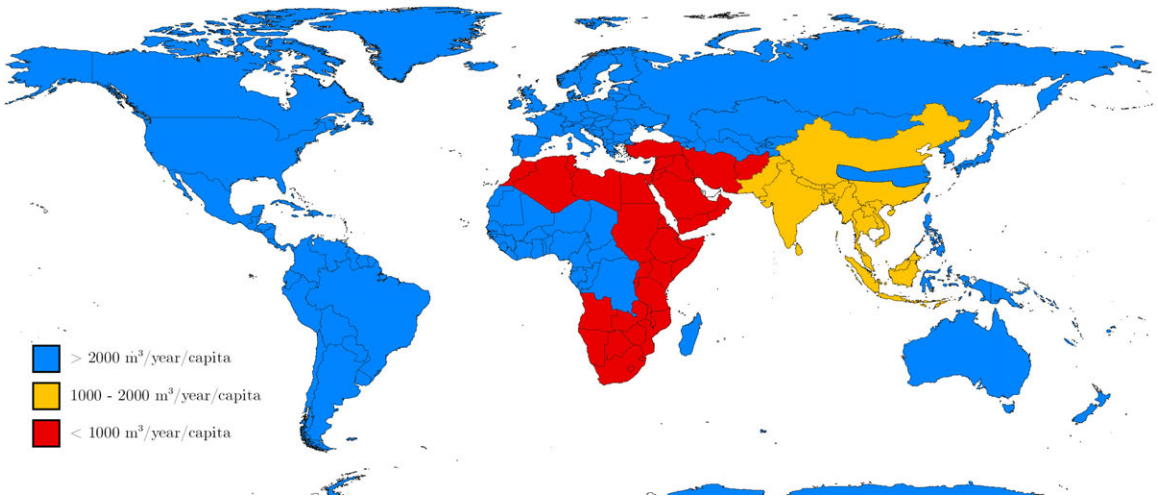

Figure 1-1: Water scarcity in 2030 based on Falkenmark Indicator [1].

1.2 Drip Irrigation

Drip irrigation is a form of irrigation that delivers water directly to the roots of the plant, decreasing water consumption for the same crop in comparison to more common and traditional methods. Drip irrigation is implemented through a network of pipes and valves installed with drippers, or emitters, that are positioned at the root zone of each plant location. The water is pumped from a well, usually through filters, and is powered either by the electrical grid or an alternative energy source. For developing countries such as India, over 45% of the land is off-the-grid, showing an increasing need for off-the-grid drip irrigation systems [9]. Although drip irrigation has been developed and tried, it is not as widely adopted as the more popular, low-hardware methods of irrigation such as flood irrigation and surface irrigation. In these methods, the water is less controlled as large amounts of water are distributed over the plants in a flooding manner.

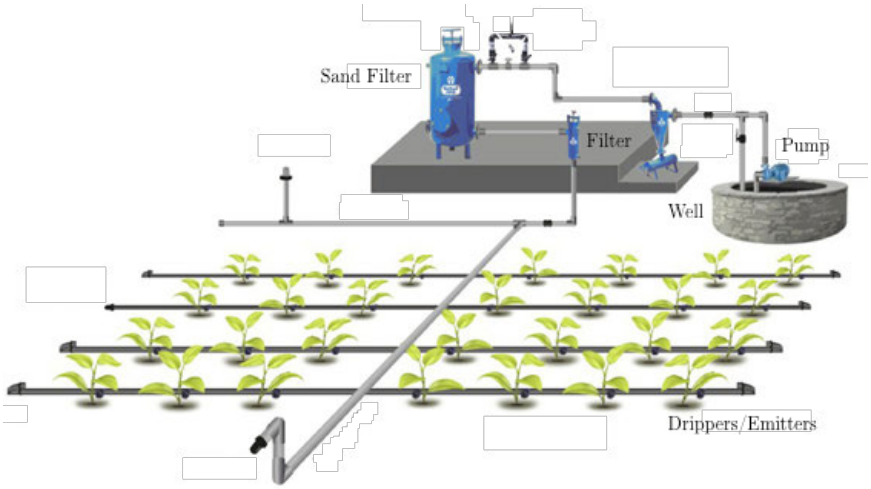

Figure 1-2: Example of a drip irrigation system layout (Photo courtesy of Plantations International Limited).

1.2.1 Advantages of Drip Irrigation

The main advantage of drip irrigation is its high water efficiency, where water efficiency is measured as the ratio between water absorbed and the total amount of water used. Studies have shown that drip irrigation can reach upwards of 95% water

efficiency as opposed to flood irrigation, which is estimated to be $40 - 50\%$ water efficiency [7, 10]. Studies have also shown that drip irrigation can reduce $30 - 50\%$ of water waste in comparison to surface irrigation. In some cases, specifically in India, drip irrigation has reduced water waste by $30 - 60\%$ while increasing crop yields by $20 - 50\%$ [7]. However, although their usage and efficiencies have been widely documented and validated, there is a barrier of entry for farmers due to initial hardware costs, even if the return on investment is within a reasonable time frame. For India, it is estimated that the return on investment in drip irrigation is realized within the first year for crops such as banana and grapes [10].

1.2.2 Solar-Powered, Drip Irrigation System

As mentioned before, for developing countries such as India, a large portion of the country is not connected to the electrical grid, making grid-based irrigation systems infeasible for a significant population [9]. Because of this demand for off-the-grid drip irrigation systems, this research will focus mainly on solar-powered drip irrigation systems. Using solar as an energy source is an attractive alternative because of its cleanliness, ubiquitousness, and relatively high reliability. However, because of the intermittency and non-constant nature of solar irradiance, which is heavily dependent on time of day and season, there is a need for some type of energy storage. This can be fulfilled through storing chemical or potential energy (i.e. a battery or an elevated water tank). In this case, the paper will refer to an elevated water tank, or buffer, as the energy storage.

1.2.3 Cost of Solar-Powered, Drip Irrigation

To increase drip irrigation adoption, the cost of solar-powered, drip irrigation must be lowered to allow for high economic accessibility. Solar-powered, drip irrigation system costs are mainly due to the photovoltaic (PV) system. In order to reduce the initial cost of these systems, the cost reduction of each individual component is key in increasing adoption. According to Swanson's Law, it is estimated that the

cost of solar panels reduce by 20% for every doubling of solar panels sold. At this current rate, costs reduce by 50% every 10 years [11]. In addition to pure hardware cost, efficiencies of emitters are key to reducing power loses, which will reduce the power needed, and in turn, reduce the cost of the hardware [12]. Although there has been previous work on improving the affordability of the individual components of the system, there has yet to be an overall system optimization.

1.3 Systems Optimization and Model

This thesis focuses on the optimization of solar-powered, drip irrigation systems to ensure the most cost effective system by taking into account cost, solar data, and water consumption data. Only by taking a comprehensive analysis into each of these inputs can a better, more cost-effective solution be reached. Currently, the cost, solar data, and water consumption data are analyzed and optimized independently. However, the optimization of each individual component does not necessarily result in a system optimization. By doing an overall system model, the optimization of system is achieved. The end result of this optimization is an output of a specific solar panel, number of solar panels, specific water pump, water buffer size, fixed tilt and azimuth angle of the solar panel, and times of operation: both start time and duration. Although the focus of this thesis is on the cost optimization, this can also be used to help farmers determine the viability of solar-powered drip irrigation in their location.

Figure 1-4 shows the overall systems model. This model uses historical solar data from the given location to help predict the amount of power available to the farmer. That data is then coupled with PV theory to estimate power output and water pump curves to estimate water output. In addition, crop-specific water consumption data are taken into account to predict the amount of deficit or surplus water at a given time step, adding that to the given water buffer size. Although there are almost infinite solutions (in terms of the output variables), there is only a small solution space that minimizes costs. The optimization loop allows the model to converge to a solution

space that minimizes cost while being practically achievable.

1.4 Case Study: Jalgaon, India

This research and analysis is based on the rural area of Jalgaon, India, a county falls below the Falkenmark and Water Resources Vulnerability Index threshold for water scarcity and stress. This region of the world also lacks snow or large season changes, making calculations more simplified. For these reason, this location was chosen.

Figure 1-3: Visual location of Jalgaon, India (Photo courtesy of Google Images).

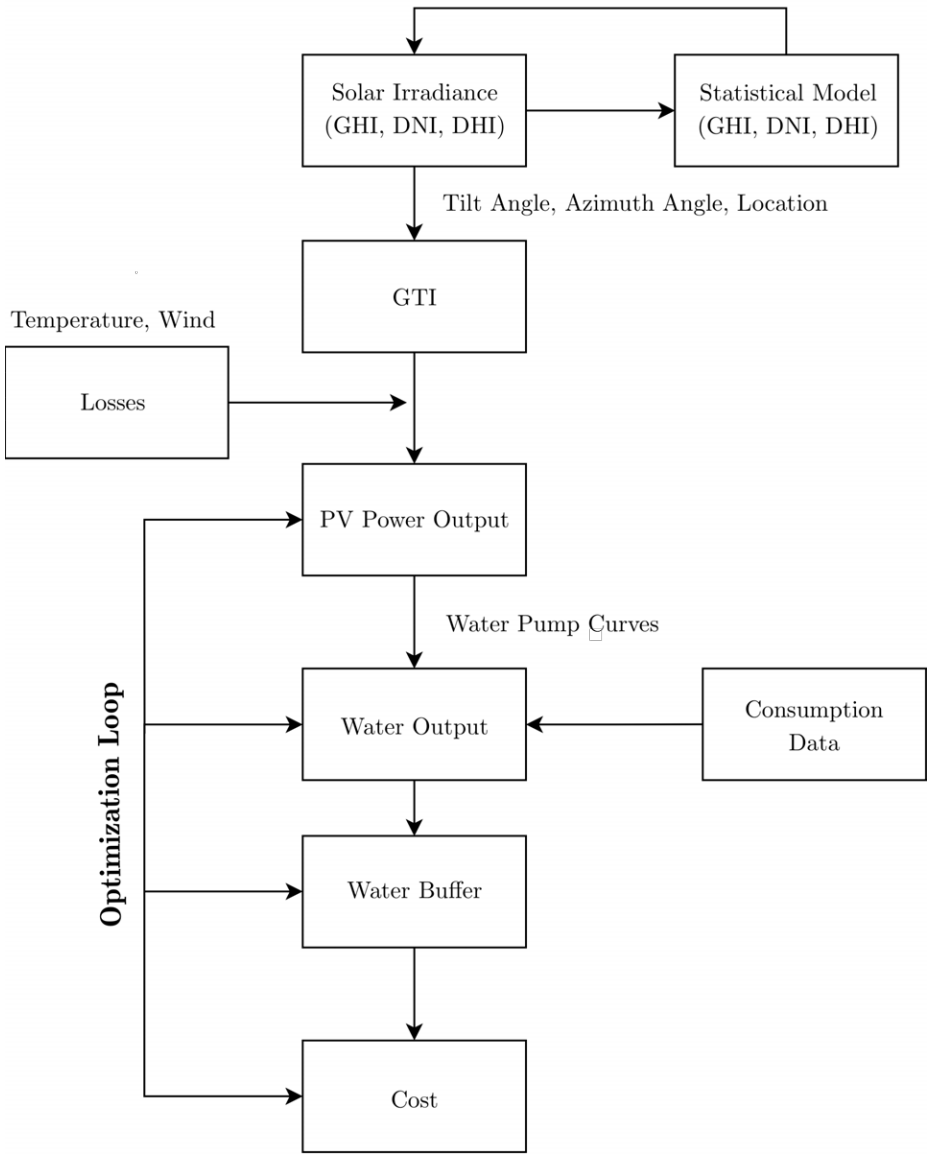

Figure 1-4: Flow chart of system design and optimization.

Chapter 2

Solar Irradiance

This section outlines the solar irradiance portion of the system model (solar irradiance, statistical model, and GTI as shown in Figure 1-4). This includes analysis of the historical solar irradiance data, the solar irradiance statistical model, and global tilt irradiance (GTI). As mentioned in the Chapter 1, in order to optimize the system, historical solar irradiance data must be analyzed to help predict future solar irradiance.

2.1 Measuring Solar Irradiance

Solar radiation is commonly measured in several metrics: Direct Normal Irradiance (DNI), Diffuse Horizontal Irradiance (DHI), and Global Horizontal Irradiance (GHI). DNI and DHI are values collected directly from radiation sensors (pyrheliometers and pyranometers). GHI can be measured through pyranometers but can also be calculated from DNI and DHI with the following relationship:

$$GHI = DHI + DNIcos\theta_z, \tag{2.1}$$

where θ_z is the solar zenith angle.

DNI is the amount of radiation received per unit area by a surface held perpendicular to the sun. DNI usually contributes the most to the total irradiance at the

surface at the PV system. DHI is the amount of radiation received per unit area on a horizontal surface. This accounts for the irradiance due to diffusion through the atmosphere and other sources that are not directly in line with the sun. GHI is the most relevant for a PV system since it accounts for both direct and diffuse radiation. However, GHI references a horizontal surface only. For most PV systems, panels are installed at a fixed angle that are greater than 0. For this use case, GHI is ill-equipped to model the amount of radiation available at the surface of the PV system. Instead, the concept of a Global Tilt Irradiance (GTI) is introduced [13, 14].

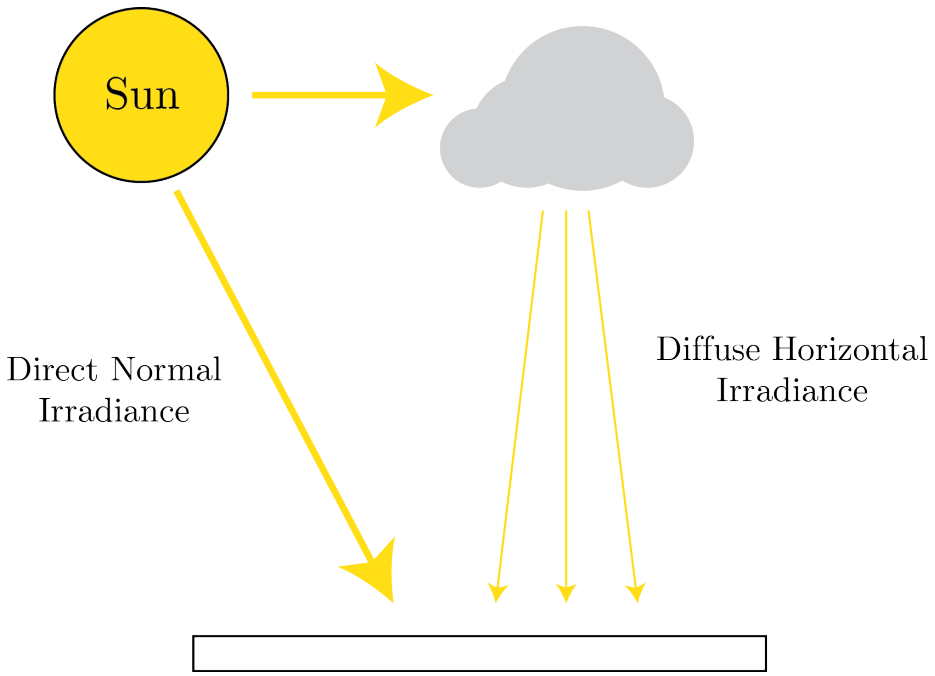

Figure 2-1: Direct normal irradiance (DNI) and diffuse horizontal irradiance (DHI) diagram.

2.2 Photovoltaic and Solar Position Angles

In order to calculate the GTI for a given PV system, several angles need to be determined. PV systems are usually rotationally determined by two angles: the tilt angle (β), which is the angle of the exposed surface relative to the ground, and the rotational angle of the PV surface (α), which is the angle relative to Earth's northern axis. Since the effective total irradiance at the surface of the PV system is dependent

on the relative difference between the surface normal of the PV and the position of the sun, or the incidence angle (θ_i), the position of the sun must be determined.

The sun position is conventionally determined by two angles: the solar zenith angle (θ_z), which is the angle of the sun relative to the zenith (the normal vector of the horizontal surface), and the solar azimuth angle (γ), which is the angle of the sun relative to the Earth's north axis. In order to determine these two angles, the Solar Position Algorithm (SPA) is utilized [15]. The complete implementation is found in Appendix A.

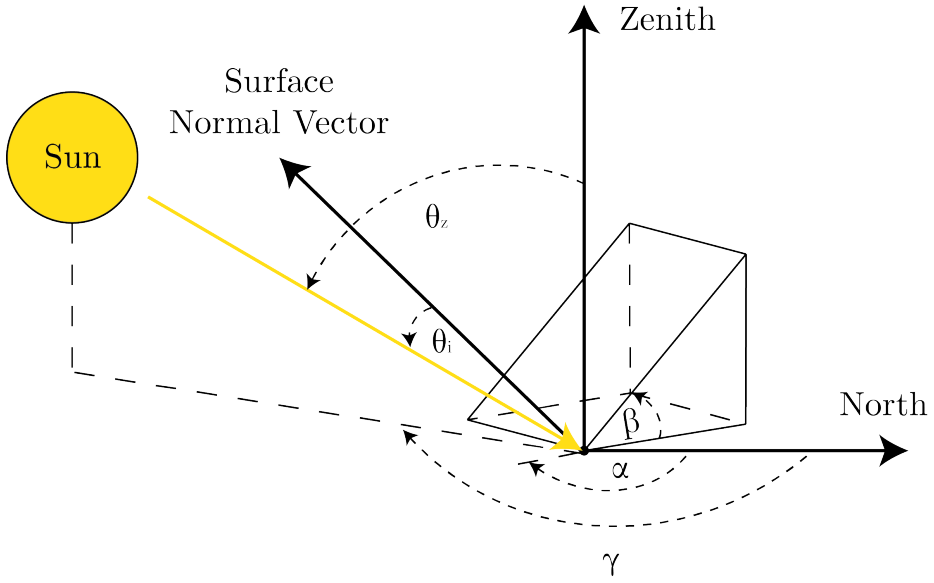

Figure 2-2: Photovoltaic and solar position angles.

2.2.1 Solar Positioning Algorithm (SPA)

As referenced in Section 2.2, several angles must be determined to accurately model the effective radiation at the PV surface for a tilted surface.Although there are several methods in which this can be done, the most accurate and documented is the SPA. The SPA takes into consideration location (latitude, longtitude, and elevation) as well as the time (year, month, day, hour, minute, second) in order to determine the sun's position. This algorithm calculates the solar zenith (θ_z) and solar azimuth angle (γ) within $\pm 0.0003^\circ$ [15].

Deviations in Length of Day (ΔT)

The SPA takes into consideration deviations in the length of day in order to more accurately model the position of the sun. Although each day only varies by milliseconds, the cumulative effect, ΔT, can effect accuracies when determining position of celestial bodies such as the sun. This phenomenon is due to the variations in the Earth's rotation as well as other causes such as lunar and solar tides [16]. Although this varies per year, a polynomial expression has been derived from historical data to help simplify evaluation of ΔT [2].

$$\Delta T = \begin{cases} 63.86 + 0.3345(t - 0.060374)t^2 + 0.0017275t^3 & 1986 \leq year \leq 2005 \\ \quad + 0.000651814t^4 + 0.00002373599t^5 & \\ 62.92 + 0.32217t + 0.005589t^2 & 2005 \leq year \leq 2050 \end{cases} \tag{2.2}$$

$$\text{where } t = year - 2000$$

Year	ΔT **(seconds)**
1990	+56.9
1995	+60.8
2000	+63.8
2005	+64.7

Table 2.1: Values of ΔT from Direct Observations [2].

2.3 Global Tilt Irradiation (GTI)

GTI is a metric that more accurately charaterizes the amount of irradiance available at the surface of a tilted PV system. Because all common measurements of irradiance refer a horizontal surface, these values need to be transformed to the frame of the tilted surface. The GTI can be divided into three categories, (i) beam tilt irradiance (B_t), (ii) diffuse tilt irradiance (D_t), and (iii) reflective tilt (R_t) irradiance [14, 17].

$$GTI = B_t + D_t + R_t \tag{2.3}$$

2.3.1 Beam Tilt Irradiance (B_t)

Beam Tilt Irradiance (B_t) is equivalent to DNI with an angle correction factor to compensate for the tilt of the solar panel and can be calculated by:

$$B_t = DNIcos\theta_i, \tag{2.4}$$

where θ_i is the incidence angle (the angle between of the normal of the PV surface and the sun beam) [14, 17].

The incidence angle can be calculated with

$$cos\theta_i = cos\theta_z cos\beta + sin\theta_z sin\beta cos(\gamma - \alpha), \tag{2.5}$$

where β is the tilt angle of the PV surface, α is the rotational angle of the PV surface, γ is the solar azimuth angle, which is the relative position of the sun to the normal of the horizontal surface, and θ_z is the solar zenith angle, which is the relative position of the sun to the normal of the horizontal surface [17].

2.3.2 Diffuse Tilt Irradiance (D_t)

Diffuse Tilt Irradiance (D_t) consists of several diffusing components: isotropic (i.e. uniform dome irradiance), circumsolar (i.e. scattering near sun area), and horizontal (i.e. concentrated scattering at the horizon). There are models, both isotropic and anisotropic, that have been developed in order to characterize D_t by using DHI and a diffusion transposition factor (F_d).

$$D_t = (DHI)F_d \tag{2.6}$$

There are several isotropic (i.e. assume uniform diffusion of sky radiation) models, such as the Liu-Jordan, Korokanis, and Badescu, as well as antisotropic (i.e. different diffusion near the sun than the rest of the sky dome) models, such as the Willmot, Bugler, Hay, Skartveit-Olseth, Temps-Coulson, and Klucher [17].

For this case, the Liu-Jordan, an isotropic model, is used to predict within 10% -

15% [18]. The Liu-Jordan model is as

$$F_d = \frac{1}{2}(1 + cos\beta), \tag{2.7}$$

where β is the tilt angle of the PV surface [17].

2.3.3 Reflective Tilt Irradiance (R_t)

Reflective Tilt Irradiance (R_t) is an additional term that accounts for reflection of radiation from the ground and can be modelled as

$$R_t = \rho(GHI)F_h, \tag{2.8}$$

where ρ is the foreground's albedo and F_h is the transposition factor for ground reflection [17]. Albedo is defined as the proportion of radiation that is reflected by a surface, and in this case, the ground. Although albedo varies throughout the year, most models assume a constant albedo, which is dependent on location [17]. In this case, an albedo (ρ) of 0.1 is assumed throughout the year.

Surface Type	**Approximate Albedo (ρ)**
Body of water	0.10
Farmland	0.15
Deserts	0.25
Snow-covered land	0.40
Snow-covered ice	0.80

Table 2.2: Approximate values of albedo (ρ) for different surfaces [3].

For the transposition factor model, many papers [13, 14] assume an isotropic model, and can be estimated to be

$$F_h = \frac{1}{2}(1 - cos\beta), \tag{2.9}$$

where β is the tilt angle of the PV surface [17].

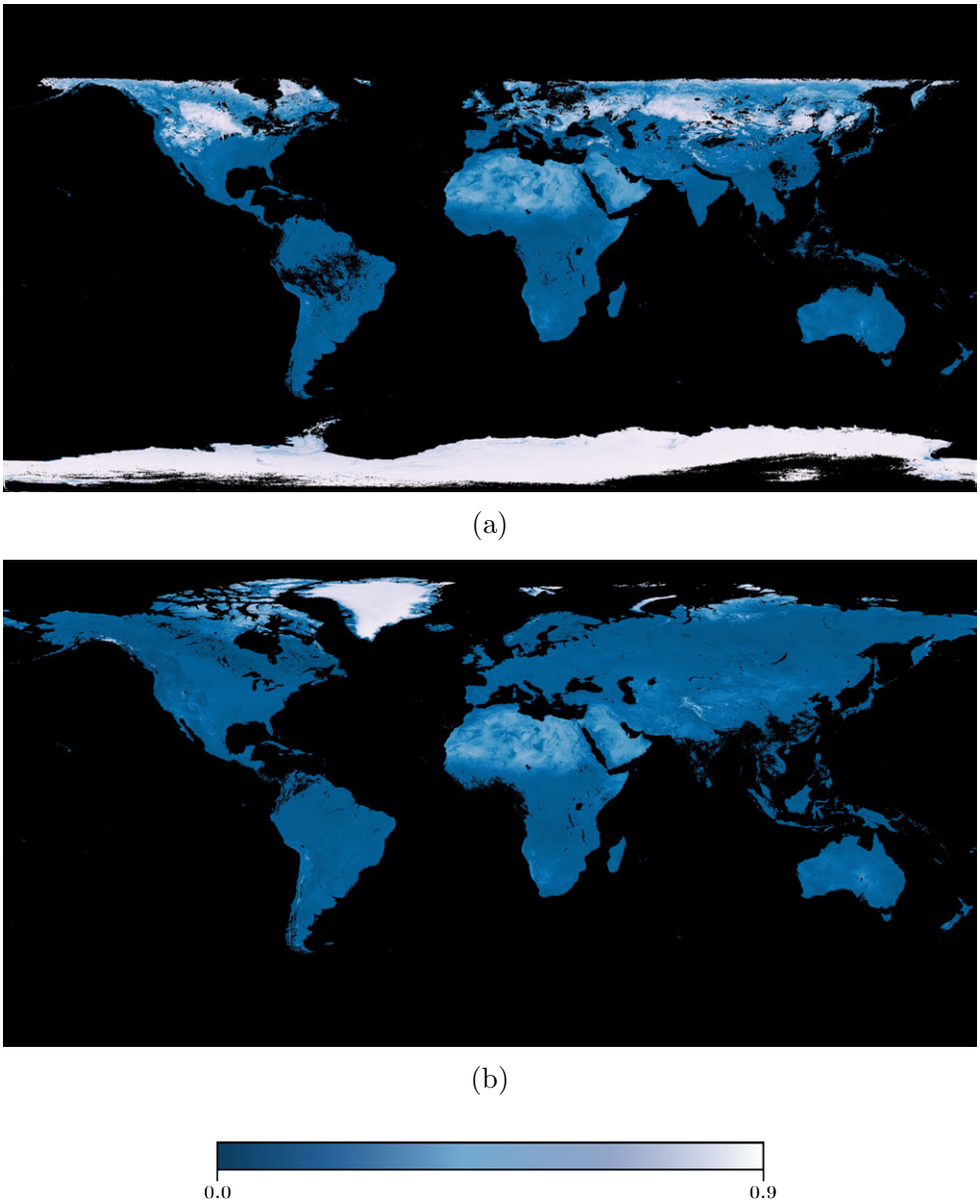

Figure 2-3: Visual snapshots of albedo in (a) January 2010 and (b) June 2010 (Photos courtesy of NASA Earth Observations).

2.3.4 Overall GTI Equation

By combining equations 2.3, 2.4, 2.5, 2.6, 2.7, 2.8, and 2.9, we can express GTI as

$$\begin{aligned} GTI = DNI[cos\theta_z cos\beta + sin\theta_z sin\beta cos(\gamma - \alpha)] \\ + \frac{1}{2} DHI(1 + cos\beta) \\ + \frac{1}{2} \rho(GHI)(1 - cos\beta). \end{aligned} \tag{2.10}$$

By inspection, as β, γ, and α approach 0 (horizontal configuration), GTI approaches GHI.

2.4 Solar Irradiance Data: Jalgaon, India

As mentioned previously in this section, in order to help predict and characterize the irradiance at this given location, historical data must be analyzed. Solar data was collected from the National Renewable Energy Laboratory (NREL) Solar Radiation Database. The location specified (Jalgaon, India) is at a latitude of 16.95°, longitude of 76.05°, elevation of 0 meters, and local time zone of 5.5 hours. The data was analyzed from 2000-2015, with hourly data points of DNI, DHI, and GHI.

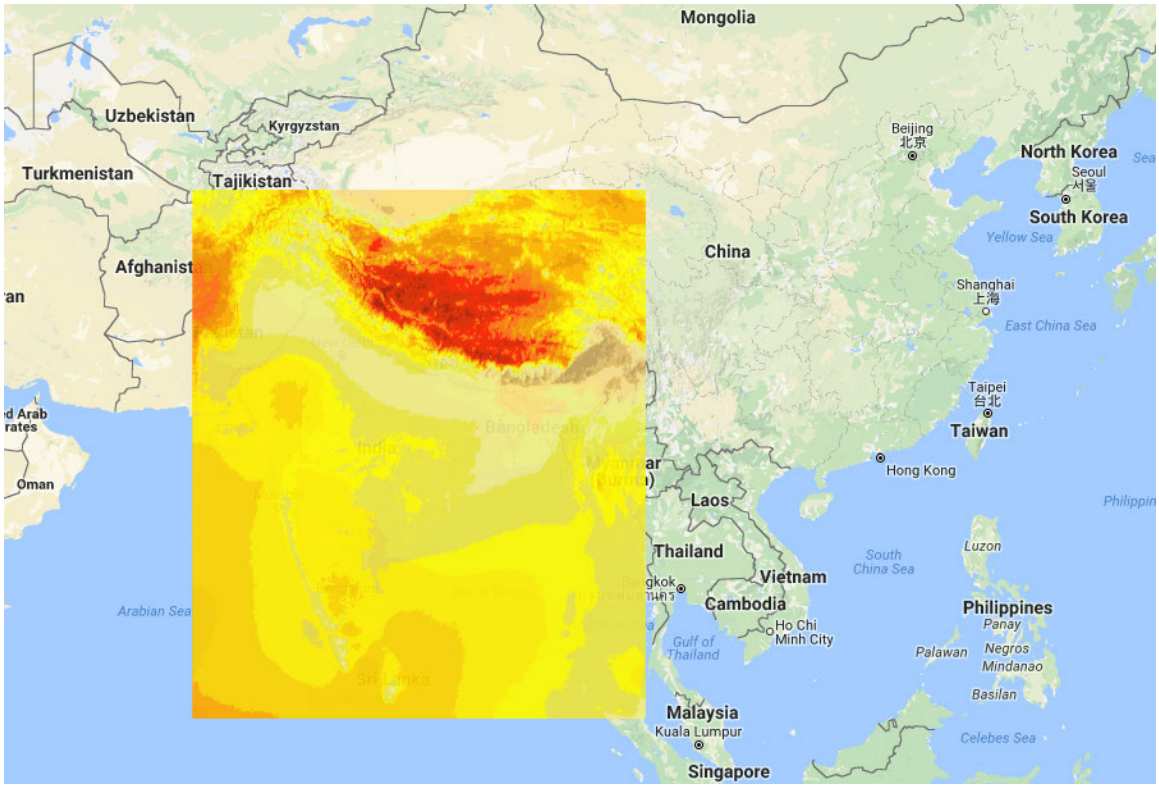

Figure 2-4: Visual of NREL database analysis tool.

Year	**Month**	**Day**	**Hour**	**Minute**	**DHI** ($\frac{W}{m^2}$)	**DNI** ($\frac{W}{m^2}$)	**GHI** ($\frac{W}{m^2}$)
2000	1	1	0	30	0	0	0
2000	1	1	1	30	0	0	0
2000	1	1	2	30	0	0	0
2000	1	1	3	30	0	0	0
2000	1	1	4	30	0	0	0
2000	1	1	5	30	0	0	0
2000	1	1	6	30	0	0	0
2000	1	1	7	30	52	90	63
2000	1	1	8	30	119	462	271
2000	1	1	9	30	159	621	476
2000	1	1	10	30	182	707	642
2000	1	1	11	30	194	751	748
2000	1	1	12	30	198	764	784
2000	1	1	13	30	244	656	727
2000	1	1	14	30	181	705	637
2000	1	1	15	30	158	617	470
2000	1	1	16	30	117	455	264
2000	1	1	17	30	40	11	42
2000	1	1	18	30	0	0	0
2000	1	1	19	30	0	0	0
2000	1	1	20	30	0	0	0
2000	1	1	21	30	0	0	0
2000	1	1	22	30	0	0	0
2000	1	1	23	30	0	0	0
2000	1	1	24	30	0	0	0

Table 2.3: Data structure of solar data collected from NREL database from Jalgaon in 2000.

2.4.1 Statistical Model

In order to account for the variation in weather from year to year, a probability density function (PDF) is fitted over the hourly irradiance data. In this case, a gaussian distribution is assumed as

$$\text{PDF}_{gauss} = \frac{1}{\sqrt{2\sigma^2 pi}} e^{-\frac{(x-\mu)^2}{2\sigma^2}}, \tag{2.11}$$

where μ is the mean of the PDF and σ is the standard deviation. The PDF returns the likelyhood of a variable, x, being randomly chosen from the given PDF. The more relevant function is the cumulative distribution function (CDF), which is the likelyhood of all values $\leq x$ being randomly chosen from the given PDF.

$$\text{CDF}_{gauss} = \frac{1}{2}[1 + \text{erf}(\frac{x-\mu}{\sigma\sqrt{2}})] \tag{2.12}$$

The imposition of a PDF will allow for a probability value to be applied to the amount of irradiance available on that hour. For example, there is a 95% probability that the irradiance on any certain hour is at least

$$\text{Irradiance}_{95\%} = \mu - 1.96\sigma. \tag{2.13}$$

By propagating the probability, mean, and standard deviation throughout the system model (from GTI to PV to Water Output to Buffer), the overall variation, and therefore, uptime of the system can be determined.

2.4.2 Calculating GTI from Solar Data

As outlined previously, to determine the GTI for a given PV system, the position of the sun must be calculated. By using location data and the date and time that correlates to the hourly solar irradiance data, the solar zenith (θ_i) and azimuth angle (γ) is calculated at each hour by using the SPA. Because these angles are constant for these specific times and dates and because the SPA is computationally intensive, the values for θ_i and γ are computed once stored in a 8760 x 16 array for all 16 years (2000-2015). Tables 2.4 and 2.5 are the result of the SPA for Jalgaon, India. By inspection, the solar zenith (θ_i) and azimuth (γ) angles are trivially different across 15 years (on the order of 0.1°) so the average for each hour of the solar zenith (θ_i) and azimuth (γ) angles is used during calculations.

From solar zenith (θ_z) and azimuth (γ) angle, along with the determined tilt (β) and azimuth (α) angle of the PV system, the overall GTI can be calculated using Equation 2.10. Since the input solar irradiance data are hourly for the entire year,

the result of the GTI calulation is a 8760 x 1 matrix output. Figures 2-5 and 2-6 are examples of GTI versus GHI for tilt (β) angles = [15°, 30°] while keeping the azimuth angle (α) = 0°.

Hour	2000	2001	2002	2003	2004	2005	2006
1	173.86°	173.92°	173.9°	173.88°	173.86°	173.92°	173.9°
2	164.38°	164.48°	164.45°	164.42°	164.38°	164.48°	164.45°
3	150.94°	151.03°	151.0°	150.97°	150.94°	151.04°	151.01°
4	137.18°	137.26°	137.23°	137.21°	137.18°	137.26°	137.24°
5	123.42°	123.49°	123.47°	123.44°	123.42°	123.5°	123.47°
6	109.78°	109.85°	109.83°	109.8°	109.78°	109.85°	109.83°
7	96.363°	96.431°	96.408°	96.387°	96.367°	96.433°	96.413°
8	83.139°	83.196°	83.176°	83.159°	83.143°	83.198°	83.181°
9	70.726°	70.771°	70.756°	70.742°	70.729°	70.773°	70.76°
10	59.244°	59.273°	59.263°	59.255°	59.247°	59.275°	59.267°
11	49.438°	49.444°	49.442°	49.441°	49.441°	49.446°	49.445°
12	42.508°	42.483°	42.492°	42.501°	42.51°	42.483°	42.493°
13	39.99°	39.929°	39.95°	39.97°	39.99°	39.928°	39.949°
14	42.673°	42.585°	42.615°	42.644°	42.672°	42.584°	42.612°
15	49.721°	49.62°	49.655°	49.687°	49.719°	49.618°	49.65°
16	59.598°	59.493°	59.529°	59.563°	59.595°	59.491°	59.524°
17	71.121°	71.018°	71.053°	71.086°	71.118°	71.015°	71.047°
18	83.555°	83.455°	83.49°	83.521°	83.552°	83.453°	83.484°
19	96.81°	96.71°	96.745°	96.776°	96.806°	96.708°	96.738°
20	110.23°	110.13°	110.17°	110.2°	110.23°	110.13°	110.16°
21	123.87°	123.78°	123.82°	123.84°	123.87°	123.78°	123.81°
22	137.64°	137.56°	137.59°	137.61°	137.64°	137.56°	137.58°
23	151.41°	151.34°	151.36°	151.39°	151.41°	151.33°	151.36°
24	164.84°	164.79°	164.81°	164.82°	164.84°	164.78°	164.8°

Table 2.4: Solar zenith angle (θ_z) during first 24 hours of the year at Jalgaon, India as calculated by the SPA.

Hour	2000	2001	2002	2003	2004	2005	2006
1	357.31°	358.09°	357.82°	357.57°	357.34°	358.11°	357.87°
2	295.6°	295.51°	295.54°	295.57°	295.61°	295.51°	295.55°
3	287.17°	287.07°	287.11°	287.14°	287.17°	287.07°	287.11°
4	285.9°	285.82°	285.84°	285.87°	285.9°	285.81°	285.84°
5	286.85°	286.77°	286.8°	286.82°	286.85°	286.77°	286.79°
6	289.02°	288.94°	288.97°	288.99°	289.02°	288.94°	288.97°
7	292.24°	292.16°	292.18°	292.21°	292.24°	292.15°	292.18°
8	296.65°	296.56°	296.59°	296.62°	296.65°	296.56°	296.59°
9	302.69°	302.59°	302.62°	302.66°	302.69°	302.59°	302.62°
10	311.12°	311.0°	311.04°	311.08°	311.11°	311.0°	311.03°
11	323.09°	322.95°	323.0°	323.04°	323.08°	322.95°	322.99°
12	339.73°	339.58°	339.63°	339.68°	339.73°	339.58°	339.62°
13	0.36288°	0.2312°	0.27642°	0.31753°	0.35702°	0.22741°	0.26692°
14	37.402°	37.366°	37.379°	37.389°	37.398°	37.364°	37.373°
15	49.237°	49.232°	49.234°	49.234°	49.234°	49.231°	49.23°
16	57.572°	57.586°	57.581°	57.575°	57.57°	57.585°	57.579°
17	63.552°	63.578°	63.57°	63.56°	63.55°	63.578°	63.568°
18	67.929°	67.966°	67.953°	67.94°	67.927°	67.966°	67.952°
19	71.119°	71.167°	71.151°	71.134°	71.118°	71.168°	71.151°
20	73.269°	73.334°	73.312°	73.289°	73.268°	73.334°	73.312°
21	74.188°	74.28°	74.249°	74.218°	74.188°	74.281°	74.25°
22	72.849°	73.0°	72.948°	72.898°	72.85°	73.002°	72.952°
23	64.033°	64.371°	64.255°	64.145°	64.037°	64.377°	64.268°
24	358.31°	359.1°	358.82°	358.58°	358.34°	359.12°	358.88°

Table 2.5: Solar azimuth angle (γ) during first 24 hours of the year at Jalgaon, India as calculated by the SPA.

As shown in the yearly GTI comparison (Figure 2-6), by changing the PV tilt angle (β), the effective irradiance achieved at the surface of the PV system can be increased during certain times, and consequently decreased during times. This is due to the fact that the tilt may cause the PV to face directly at the sun during certain seasons and face away from the sun in subsequent seasons.

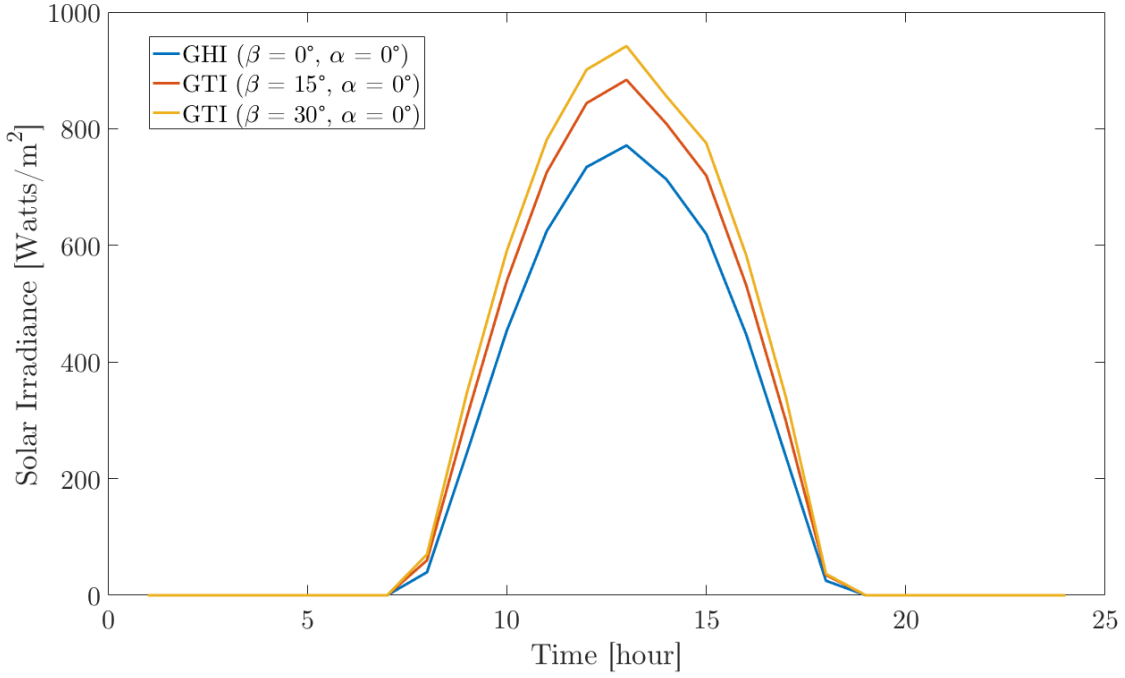

Figure 2-5: Daily GTI for PV tilt angle (β) = 0°, 15°, 30° and PV azimuth angle (α) = 0° based on data from Jalgaon, India in 2000.

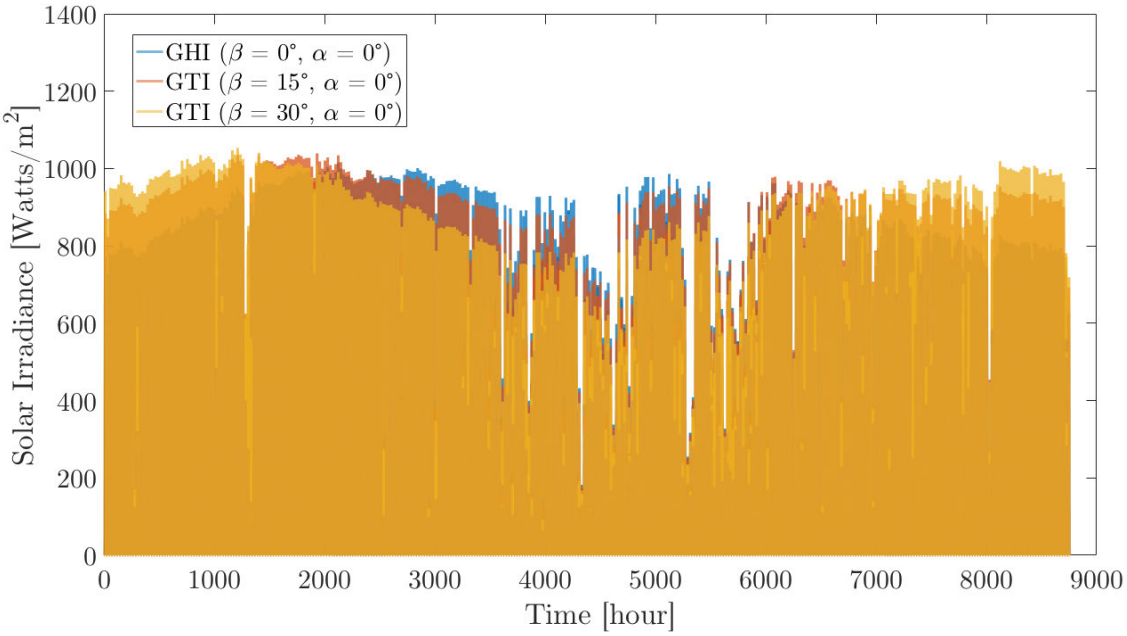

Figure 2-6: Yearly GTI for PV tilt angle (β) = 0°, 15°, 30° and PV azimuth angle (α) = 0° based on data from Jalgaon, India in 2000.

Chapter 3

Photovoltaic Power and Losses

This section outlines the PV power output and losses portion of the system (losses and PV power output as shown in Figure 1-4). This includes the translation between GTI to available power. By using the calculated GTI and accounting for several powerlosses, an estimated power output can be determined using common, available manufacturer specifications.

3.1 Solar Panel Specifications and Power Output

A database of solar panels with specifications such as Nominal Power (W_p), Module Efficiency (η_{ref}), Temperature Coefficient (β_{ref}), Effective Area (A_{eff}), and Cost per Watt ($\$/Watt$) was aggregated from popular solar panel distributors.

The standard for measuring nominal power (W_p) of solar panels is dictated by the International Electrotechnical Commission (IEC). Generally, the power output is measured as the DC output of the panel at Standard Testing Conditions (STC). STC consists of a constant irradiance of 1000 Watts/m^2, temperature of 25°C, and air mass of 1.5.

In order to estimate the power output of the solar panel given a non-nominal irradiance

$$P_{output} = (GTI)A_{eff}\eta_c. \tag{3.1}$$

		AE Solar	Suntech Power
		AE305M672	**STP290S20Wew**
Nominal Power	$P_m(W_p)$	305	290
Open-circuit voltage	V_oc (V)	45.58	39.8
Short-circuit current	I_sc (A)	8.83	9.55
Voltage at max power	V_mp(V)	38.23	31.7
Current at max power	I_mp (A)	7.98	9.15
Module efficiency	η_{ref} (%)	15.77	17.8
Temp coefficient	β_{ref} (%/°C)	-0.36	-0.4
NOCT	°C	45	45
Dimensions	L (mm)	1950	1640
Dimensions	W (mm)	992	992
Dimensions	H (mm)	40	35
Type of cell		mono	mono
Cost	($/$W_p$)	0.439	0.395
Effective Area	(m^2)	1.93	1.63

Table 3.1: Manufacturer specifications of several PV modules in the solar panel database.

3.2 Power Losses

To more accurately model the power output of the solar panel, power losses must be accounted. Power losses are inefficiencies within the system or interfaces between systems that reduce the ideal available power as calculated in Equation 3.1. These power losses are due to the following:

1. Array Incidence Losses
2. Thermal Cell Losses
3. Real Module Performance Losses
4. Mismatch Losses
5. Dirt/Dust Losses
6. Ohmic Losses

3.2.1 Array Incidence Losses

Array incidence losses due to the surface interaction between the solar irradiance and PV module surface (i.e glass reflection). The incidence effect corresponds to the decrease of irradiance that reaches the PV cell due to reflection of the glass layer. In theory, the Fresnel reflection and Snell's law can be used to characterize the incidence angle effects on an air- glass interface. However, empirical methods to measure the effect of angle on cell irradiance absorption provide more accurate analytical solutions and is specified in ASHRAE Standards 93-77 [19]. The incident angle modifier (IAM) is used in this standard to characterize this reflection loss. The correction factor is applied to the incoming GTI to compensate for the reduction in irradiance reaching the cell [20].

$$GTI_{actual} = (IAM)GTI_{normal} \tag{3.2}$$

where the IAM is determined to be

$$IAM = 1 - b_0[sec(\theta_i) - 1], \tag{3.3}$$

where b_0 is assumed to be 0.05, θ_i is the incidence angle, and GTI_{actual} is the global tilt irradiance after accounting for losses of GTI_{normal} [20, 21, 22]. Because $sec(\theta_i)$ is essentially unbounded and can range from [-∞ -1] $\bigcup$ [1 ∞], the overall IAM is bounded between [0 1].

3.2.2 Thermal Cell Losses

Thermal cell losses are due to decreased performance as the cell temperature deviates from STC. Generally, solar cell performance decreases linearly with increasing temperature (using the temperature coefficient (P_m) due changes at the molecular level. To determine the temperature of the cell, there are correlations expressing the PV cell temperature (T_c) as a function of weather such as ambient temperature (T_a), local wind speed (v_{wind}), and solar irradiance (GTI), accounting for material and system

properties (i.e. plate absorption (α_{absorb})).

Most PV modules convert approximately 6-20% of the solar irradiation into electricity, depending upon the type of solar cells and environmental conditions. The other 80% of the irradiation is converted into heat, which significantly increases the temperature of the PV cell and therefore decreases the efficiency of the PV module. The temperature of the cell can be determined by an energy balance between ambient temperature and the cell's temperature due to irradiance absorption [22, 23]

$$U(T_c - T_{amb}) = \alpha_{absorb} GTI(1 - \eta_c), \tag{3.4}$$

where U is the effective heat transfer coefficient, α_{absorb} is the absorption coefficient, η_c is the cell efficiency, T_c is the cell temperature, and T_{amb} is the ambient temperature. U can be split into a natural convection term (U_{nc}) and a forced convection term (U_{fc}) (i.e. due to wind (v_{wind})) where

$$U = U_{nc} + U_{fc} v_{wind}. \tag{3.5}$$

The efficiency of the cell (η_c) can be calculated as

$$\eta_c = \eta_{ref}[1 - \beta_{ref}(T_c - T_{ref})], \tag{3.6}$$

where β_{ref} is the temperature coefficient specified by the manufacturer and $T_{ref} = 25°C$ (STC) [24].

Combining Equations 3.4, 3.5, and 3.6, the overall equation for determining η_c is

$$\eta_c = \frac{\eta_{ref}\Big[1 - \beta_{ref}\big[\frac{\alpha_{absorb}\mathrm{GTI}}{U_{nc} + U_{fc} v_{wind}} + T_{amb} - T_{ref}\big]\Big]}{1 - \frac{\eta_{ref}\beta_{ref}\alpha_{absorb} GTI}{U_{nc} + U_{fc} v_{wind}}}. \tag{3.7}$$

For the heat transfer coefficients, $U_{nc} = 29\frac{W}{m^2 K}$, $U_{fc} = 0\frac{Ws}{m^3 K}$, and $\alpha_{absorb} = 0.9$ was used for a free standing array [22].

3.3 Real Module Performance Losses

Real module performance losses are due to deviation of the module performance compared to the manufacturer's specifications. To achieve a confidence interval of 95%, the tolerance (σ) on power output is used as the standard deviation and the nominal value ($P_{nominal}$) as the mean.

$$P_{out} = P_{nominal} - 1.96\sigma \tag{3.8}$$

3.3.1 Mismatch Losses

Mismatch losses are due to the fact that in a string of modules, the lowest current dictates the system current. This is due to small variations between each module or cell. Because the mismatch losses are dependent on each specific PV system, this study assumes a 2% loss [22].

3.3.2 Dirt/Dust Losses

Dirt/dust losses are due to dirt, dust and other particles that cover the surface of the PV module. Although typical dust particles are on the order of 10μm in size, they can accumulate over time. The amount of accumulated dust on the surface of PV modules can affect the overall power output on a daily, monthly, seasonal, and annual basis.

Studies have indicated an average daily efficiency reduction of 0.2% in days without rainfall in dry weather [25]. Annual losses caused by this trend due to soiling ranges from 1.5% to 6.2% depending on the location of the PV. In this study, these losses are assumed to be 3%.

3.3.3 Ohmic Losses

Ohmic losses refer to heat losses (IR^2) in the wiring of the PV system. These losses can be characterized by the wire resistance (R) of the entire PV system. The value of

R can be calculated using american wire gauge standard tables with an assumption about wire lengths. In this study, the ohmic losses are assumed to be 3%.

As shown in Figures 3-1 and 3-2, the losses are non-trivial, especially when attempting to accurately model available power output.

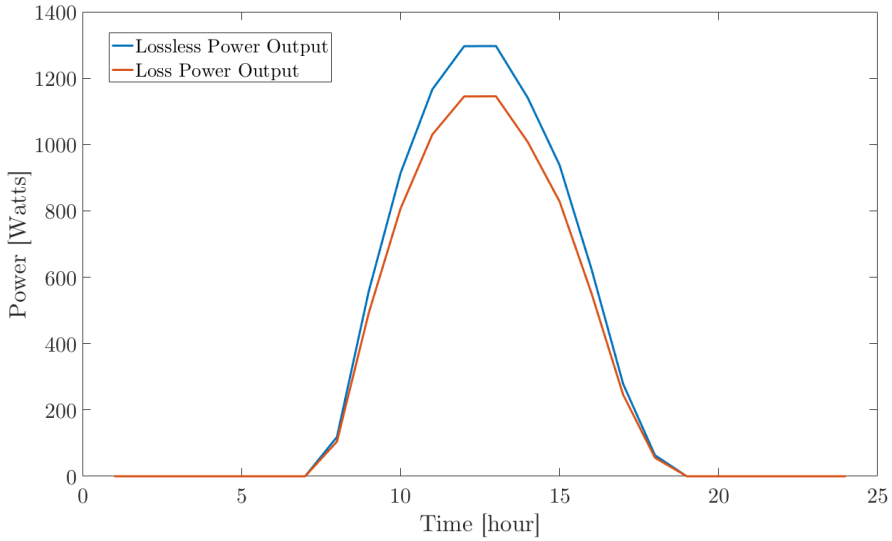

Figure 3-1: Power output losses for an arbitrary PV system over the first 24 hours based on data from Jalgaon, India in 2000. This example assumed a ΔT of 10°C and no real module performance losses.

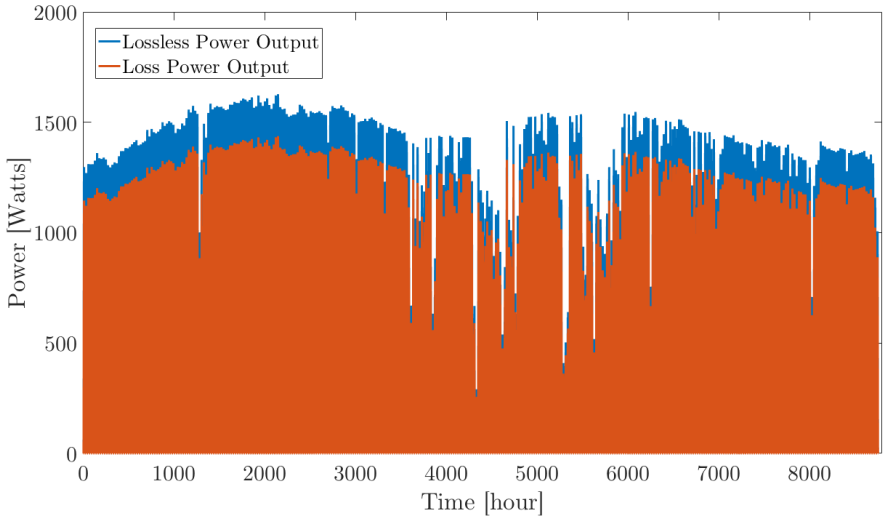

Figure 3-2: Power output losses for an arbitrary PV system based on data from Jalgaon, India in 2000. This example assumed a ΔT of 10°C and no real module performance losses.

Chapter 4

Water Consumption, Output and Buffer

This section outlines the water consumption, output, and buffer portion of the system (consumption data, water output, and water buffer as shown in Figure 1-4). This includes the analysis of specific-plant water consumption data as well as calculating the expected water output given water pump curves and PV power input.

4.1 Water Consumption

To model the rate of water needed per hour for the entire year, consumption data are taken empirically from the field for plants such as barley, wheat, and tomatoes. Data were collected from the Food and Agriculture Organization (FAO) of the United Nations (UN). Crop water consumption data are normally structured as seen in Table 4.1 and 4.2.

The periods (initial, development, mid-season, late-season) refer to the crop's progress from initial plant to harvesting. The initial period is from initial sowing to the crop has ˜10% ground coverage. The development period refers to the stage between the end of the initial period to full ground cover (˜70-80%). The mid-season refers to the stage between the end of the development period to full maturity. The late-season refers to the stage between the mid-season period to harvest [26].

	Total Days	**Initial**	**Dev**	**Mid-season**	**Late-season**
Barley	120	15	25	50	30
Oats	120	15	25	50	30
Wheat	120	15	25	50	30
Peanut	130	25	35	45	25
Sunflower	125	20	35	45	25
Tomato	135	30	40	40	25

Table 4.1: Length (in days) of stages for different plants. Data are provided by the Food and Agriculture Organization (FAO) of the United Nations.

	Initial	**Dev**	**Mid-season**	**Late-season**	**Total Water**(mm)
Barley	0.35	0.75	1.15	0.45	650
Oats	0.35	0.75	1.15	0.45	650
Wheat	0.35	0.75	1.15	0.45	650
Peanut	0.45	0.75	1.05	0.70	700
Sunflower	0.35	0.75	1.15	0.55	1000
Tomato	0.45	0.75	1.15	0.80	800

Table 4.2: Single crop coefficient (K_c) values for different plants during different periods. Data are provided from the Food and Agriculture Organization (FAO) of the United Nations.

The single crop coefficient (K_c) is a crop specific correction factor that takes into consideration climate during certain crop periods. The water needed, or evapotranspiration, refers to the depth of water absorbed, evaporated, or otherwise lost per day for the given crop. In other words, it is the amount needed by the specific crop to grow optimally under optimal conditions (i.e. uniform crop, complete ground shading, disease free). This value is usually measured through an evaporation pan in which a crop is submerged with a known volume of water. After 24 hours, the height of the water is measured [26].

Total consumption rate per season can be modelled as

$$Q_{consump} = K_c Q_{need} Area_{crop}. \tag{4.1}$$

Because the data are based on growing seasons, it is assumed that the water consumption across days in the same periods are equal. It is also assumed that the consumption rate during the day is evenly divided across the hours of operation of

the irrigation system.

4.2 Water Output

Water output is dependent on the specific water pump that is used with the drip irrigation system. Since the pump is PV driven, the water pump curves, which describe the relationship between power and water output, is used to help model the amount of water produced at a given time.

A database of water pumps was aggregated from popular water pump manufacturers (i.e. Lorentz, Grunfos). Because the power consumption (P_{in}) versus water output (Q_{out}) curves for the given pump is commonly in graph form, several data points are extracted from the curve. From those data points, linear interpolation is used to estimate water output between data points. Because of the nature of the curve, this is a conservative estimate since it undershoots the real value. Using the power output of the PV system as the power consumption (P_{in}), water output can be estimated.

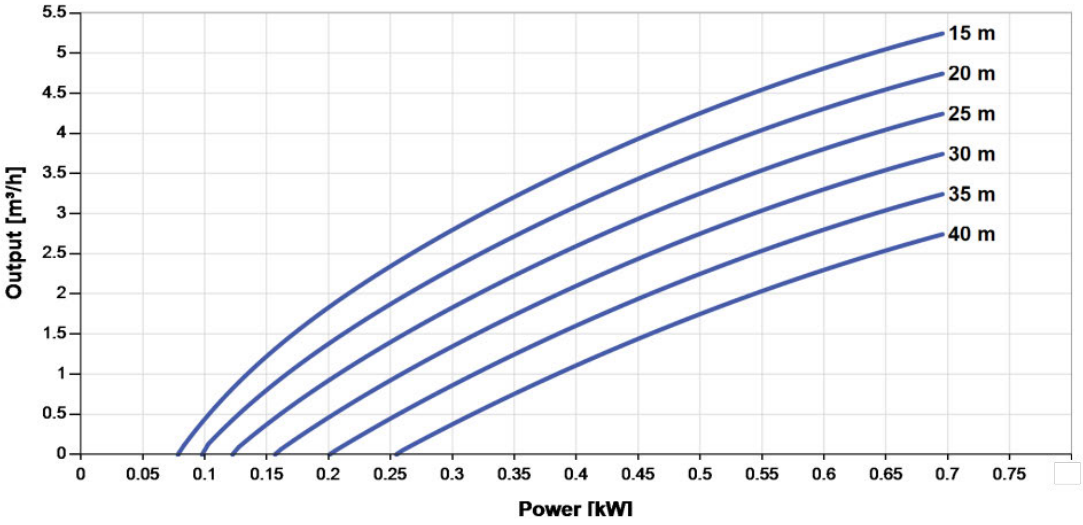

Figure 4-1: Example pump curve for Lortenz PS600 CS-F3-7 water pump.

4.3 Water Buffer

Due to the intermittency and non-constant value of solar irradiance, a water buffer is used in order to help smooth out water in and water out. This is commonly done in order to ensure that crop consumption can be fulfilled throughout the year without an unreasonable amount of solar panels. To predict the amount of excess or lack of water available at a certain time, the equation can be expressed as

$$Q_{total} = Q_{out} - Q_{consump}. \tag{4.2}$$

This value can then be added to the water buffer ($V_{buffer}(t)$), to determine the current water buffer size.

$$V_{buffer}(t) = Q_{out} - Q_{consump} + V_{buffer}(t-1) \tag{4.3}$$

Generally, the buffer (V_{buffer}) should never reach below 0 or there will not be enough water to fulfill the water consumption needed for the specific crop.

The relationship between water output, consumption rate, and buffer size as a function of time can be shown in Figure 4-2.

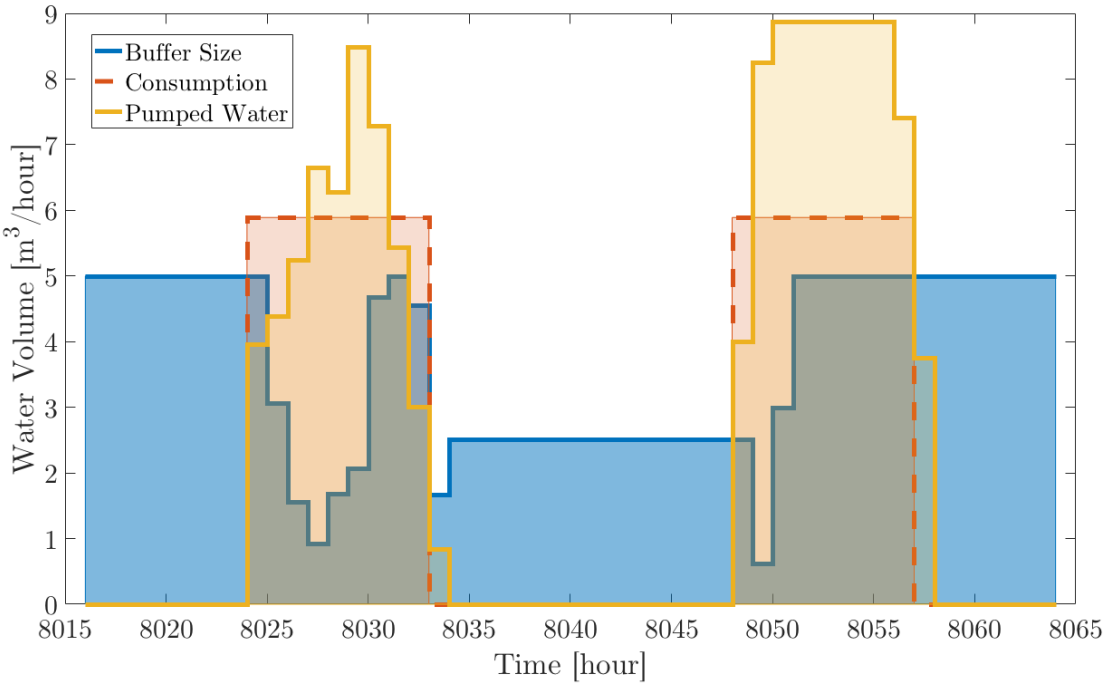

Figure 4-2: Buffer size (blue line), consumption (dotted red line), and water output (yellow line) are shown, describing the change in these variables as a function of time over two consecutive days for one acre of tomato plant. This is based on solar irradiance data from Jalgaon, India in 2000 using arbitrary solar panels and water pump.

Chapter 5

Optimization

This section outlines the optimization portion of the system. This includes the design variables, constraints, and objective function of the algorithm. In order to increase economic accessibility to drip irrigation systems as mentioned in the introduction, a cost optimzation of the entire system (solar panels, water pump, water buffer size) must be completed.

Most current research and papers optimizing the tilt angle (α) and azimuth angle (β) of solar panels are focused on maximizing overall power output throughout the entire year. However, although this is applicable for PV systems feeding into a power grid, α and β optimization of solar panels for a drip irrigation system does not necessarily coincide with the tilt and azimuth angle for maximum power output. This is due to the possibility that the α and β will be optimized to maximize water output during times of high water consumption, low buffer, or low irradiance in the case of different crops.

5.1 Genetic or Evolutionary Algorithms

For the optimization of this system, a genetic (or evolutionary) algorithm (GA) was chosen. GA is a stochastic method of solving both constrained and unconstrained optimization problems based on natural selection. Each generation contains a population of individual solutions. At each iteration, the algorithm chooses from the

current population and uses it to produce children for the next iteration. Over many generations, the population trends towards an optimal solution. Because this method is stochastic, it is computationally more demanding than gradient decent methods and does not necessarily guarantee the most optimal solution. One of the advantages of this algorithm method is that it can account for non-continuous variables, such as the selection of the solar panels, number of solar panels, and selection of the water pump (as integers in a database). The GA can be divided into several categories: the objective function, objective constraints, objective variables, stopping criteria.

5.1.1 Objective Variables

For this model, there are eight total design variables:

1. Number of solar panels (N_{solar})
2. Water buffer size (V_{buffer}) [m^3]
3. Tilt angle (α) [$^\circ$]
4. Azimuth angle (β) [$^\circ$]
5. Specific solar panel (i_{panel})
6. Specific water pump (i_{pump})
7. Start time (t_{start})
8. End time (t_{end})

5.1.2 Objective Function

The objective function is the function that the GA is trying to minimize or maximize. In this case, the cost (in USD) is being minimized and can be represented as

$$\text{Objective} = min(Cost_{solar} + Cost_{buffer} + Cost_{pump} + Cost_{irrigation}), \tag{5.1}$$

where the cost of each component can be broken down to the following:

$$Cost_{solar} = \frac{\$}{W} W_p N_{solar} \tag{5.2}$$

$$Cost_{buffer} = \frac{\$}{m^3} V_{buffer}$$

$$\frac{\$}{m^3} = \begin{cases} \$150 & 0 \leq V_{buffer} \leq 10 \\ \$250 & V_{buffer} > 10 \end{cases} \tag{5.3}$$

$$Cost_{pump} \approx \$1000 \tag{5.4}$$

$$Cost_{irrigation} \approx \$1250 \tag{5.5}$$

As shown in the previous equations, the objective function is only directly dependent on two objective variables, V_{buffer} and N_{solar}. Other variables, such as the specific solar panel, tilt angle, and azimuth angle drive are driving the objective variables through the objective constraint function.

5.1.3 Objective Constraint

The objective constraint function allows for the solution space to be limited by certain physical and practical factors (i.e. the number of solar panels is an integer number).

In this case, there is one major objective constraint:

$$min[V_{buffer}(t)] \geq 0. \tag{5.6}$$

This constraint is due to the physical requirement that V_{buffer} must always be greater than zero or the system would not fulfill the desired water consumption rate.

The water buffer is a function of time, which is dependent on the current buffer (V_{buffer}), water output (Q_{out}), and consumption rate ($Q_{consump}$) as described in Equation 4.3. However, since the water buffer size cannot exceed the initial V_{buffer}, the

equation is bounded as

$$V_{buffer}(t) = \begin{cases} V_{buffer}(t-1) + Q_{out} - Q_{consump} & V_{buffer}(t) < V_{buffer} \\ V_{buffer} & V_{buffer}(t) \geq V_{buffer} \end{cases} \tag{5.7}$$

In addition to the major objective constraint, a constraint on start time (t_{start}) and end time (t_{end}) is enforced to ensure it is physically possible.

$$t_{start} < t_{end} \tag{5.8}$$

Integer and Limit Constraints

GA allows for non-continuous functions and therefore, integer constraints can be applied to any of the design variables.

Because the specific solar panel and specific water pump variables are based off indices in a matrix or database, the design variables are constrained to integer values, which are bounded between [0 length(DB)]. In addition, the number of solar panels (N_{solar}) can only physically be integers.

In order to restrict the solution space even further, the integer constraint is also applied to the tilt angle (α) and the azimuth angle (β) since installations will not be accurate within 1°. α is bounded between [0 90] since all other angles would be trivial (i.e. the PV module facing the ground) while β is bounded between [0 360].

The objective constraint function is the most computationally rigorous due to the constant recalculating of the GTI, Q_{out}, and V_{buffer} for every set of possible solution. This function must be run for every individual in a population, which can contain thousands of different combinations. To decrease the run time, as described before, the SPA is averaged across the available years and stored rather than recalculated every iteration.

5.1.4 GA Stopping Criteria

Since there is no guarantee or confirmation that the minimum point is found, there needs to be an applied stopping criteria that determines if the algorithm is completed. To do so, there are several metrics: total generations limit, time limit, fitness limit, stall generations limit, and functional tolerance limit.

Total generations limit stops the GA after exceeding a certain amount of generations. Time limit stops the GA after a certain amount of run time. Fitness limit stops the GA after the objective function (or fitness function) decreases below a certain value. Stall generations limit stops the GA after a certain amount of iterations without observing a change in the objective function greater than the functional tolerance. For this thesis, stall generation and total generation limits were imposed.

Chapter 6

Optimization Parameters and Results

As mentioned in the introduction, Jalgaon, India will be used as an case study to run the optimization as described in the previous chapters. In this case, the 2000 solar irradiance data were used as the baseline with several crops (assumed 1 acre of crop): sunflowers, tomatoes, and barley. The optimization was run in parallel pools using an Intel Haswell Core i5-4590 3.3Ghz Quad-Core processor.

6.1 Optimization Parameters

As mentioned in Chapter 5, there are many parameters and limits applied to the design variables. The design variables can be described as an array:

$$x = [N_{solar}, V_{buffer}, \alpha, \beta, i_{panel}, i_{pump}, t_{start}, t_{end}]. \tag{6.1}$$

6.1.1 Limit and Integer Constraints

The following are the limits applied to the variables:

$$l = \Big[[0\ 1000], [0\ 100000], [0\ 90], [0\ 360], [0\ \text{length}(DB_{PV})], \\ [0\ \text{length}(DB_{pump})], [0\ 24], [0\ 24]\Big] \tag{6.2}$$

For number of solar panel and buffer size, a upper limit of 1000 and 100000 was placed to reduce the solution space.

In addition to limit constraints, all variables were integer constrained to prevent fractional numbers and non-existing database indices.

6.1.2 Stopping Criteria

The following were the stopping criteria parameters on the algorithm:

Total Generation	5000
Stall Generation	500
Functional Tolerance	1

Table 6.1: Stopping criteria for GA.

Although the convergence of different crops may be much shorter, the stall generation is set to 500 to better ensure that a local minimum was not reached.

6.2 Results

For each crop, the optimization was run three times to observe objective function convergence.

6.2.1 Crop: Sunflowers

	Run 1	**Run 2**	**Run 3**
N_{solar}	5	5	5
V_{buffer} (m^3)	5	6	5
α $(^\circ)$	14	28	16
β $(^\circ)$	287	327	302
i_{panel}	CS6X310P	STP300S20Wew	CS6X310P
i_{pump}	PS600 CS-F4-3	PS600 CS-F4-3	PS600 CS-F4-3
t_{start}	8	8	8
t_{end}	16	16	16
Cost ($)	4,600	4,625	4,600
Runtime (sec)	–	–	–

Table 6.2: Results of GA for sunflowers.

As shown in Table 6.2, the objective function converges to approximately $4,600, with Run 2 yielding a cost slightly larger Run 1 and Run 3. This can be contributed to the GA not necessarily finding to a global minimum.

Although Run 1 and Run 3 converge to the same cost and have the same N_{solar} and V_{buffer}, their α and β are slightly different. This is due to the fact that the water output fairly insensitive to α and β. It is shown through post processing that α can vary by several degrees and that β can vary by tens of degrees while maintaining within all objective constraints.

Water Buffer (V_{buffer}) Analysis

The major objective constraint is to keep $V_{buffer} \geq 0$ for the entire year. In order to do a sensitivity analysis, the buffer size as a function of time was analyzed.

As shown in Figure 6-1, the buffer is heavily utilized, especially towards the beginning and end of the year. That being said, it is always stays above 0, fulfilling the

objective constraint.

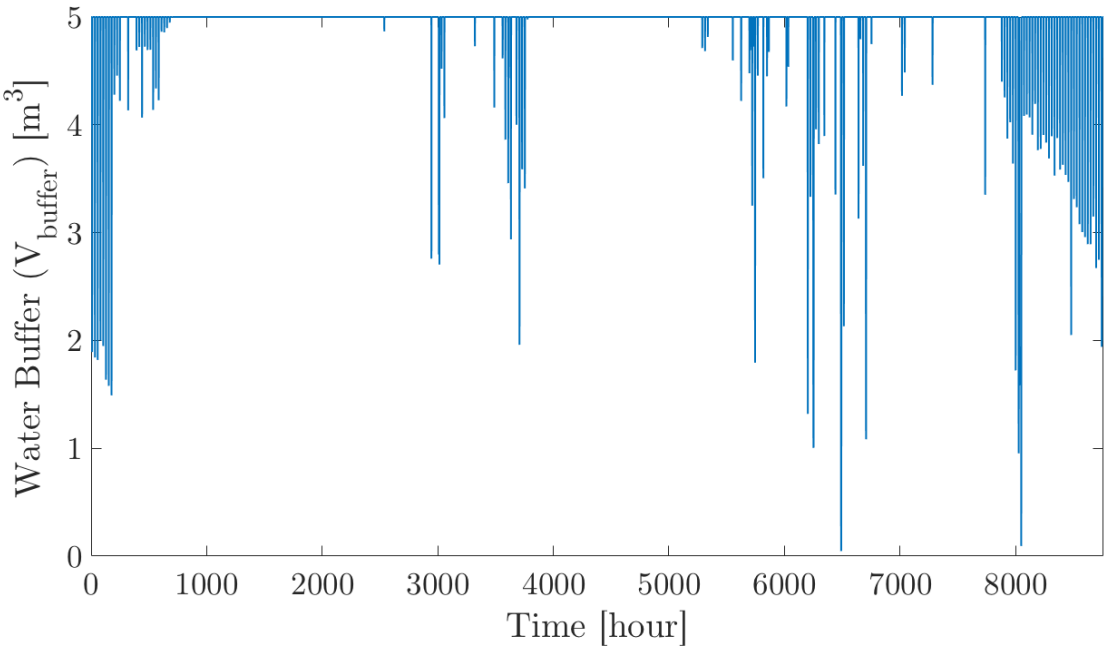

Figure 6-1: Buffer size as a function of time for the design solution of sunflowers (run 1).

Populations and Stopping Criteria

As shown in Figure 6-2, the GA stopped due to the stall generation, meaning that the algorithm could not produce a better solution for 500 generations. Technically, the first "best" solution was found within 100 generations.

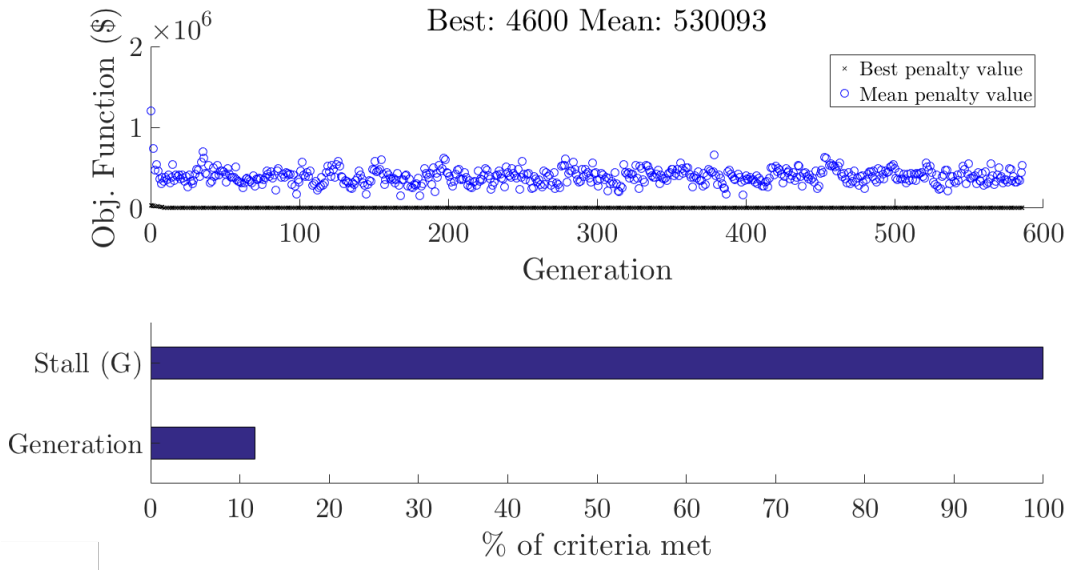

Figure 6-2: Best objective function per population and stopping criteria for sunflowers (Run 1). Each generation plots a mean objective value (blue circles) and best objective value (black x marks).

6.2.2 Crop: Tomatoes

	Run 1	**Run 2**	**Run 3**
N_{solar}	3	3	3
V_{buffer} (m^3)	5	5	5
α $(^\circ)$	2	11	2
β $(^\circ)$	258	27	274
i_{panel}	STP295S20Wew	STP295S20Wew	STP295S20Wew
i_{pump}	PS600 CS-F4-3	PS600 CS-F4-3	PS600 CS-F4-3
t_{start}	9	9	9
t_{end}	16	17	16
Cost ($)	3,870	3,870	3,870
Runtime (sec)	–	3,758	3,498

Table 6.3: Results of GA for tomatoes.

As shown in Table 6.3, the objective function Run 1, 2, and 3 converged to $3,870. Although these runs had the same N_{solar} and V_{buffer}, their α and β is slightly different. As mentioned before this is due to the fact that the water output fairly insensitive to α and β. In this case, it is also shown that α can vary by several degrees and that β can vary by tens of degrees while maintaining within all objective constraints (as

shown in the various α and β values for the same design variables).

Water Buffer (V_{buffer}) Analysis

The major objective constraint is to keep $V_{buffer} \geq 0$ for the entire year. In order to do a sensitive analysis, the buffer size as a function of time was analyzed.

As shown in Figure 6-3, the buffer is heavily utilized, especially towards the middle and end of the year. That being said, it is always stays above 0, fulfilling the objective constraint.

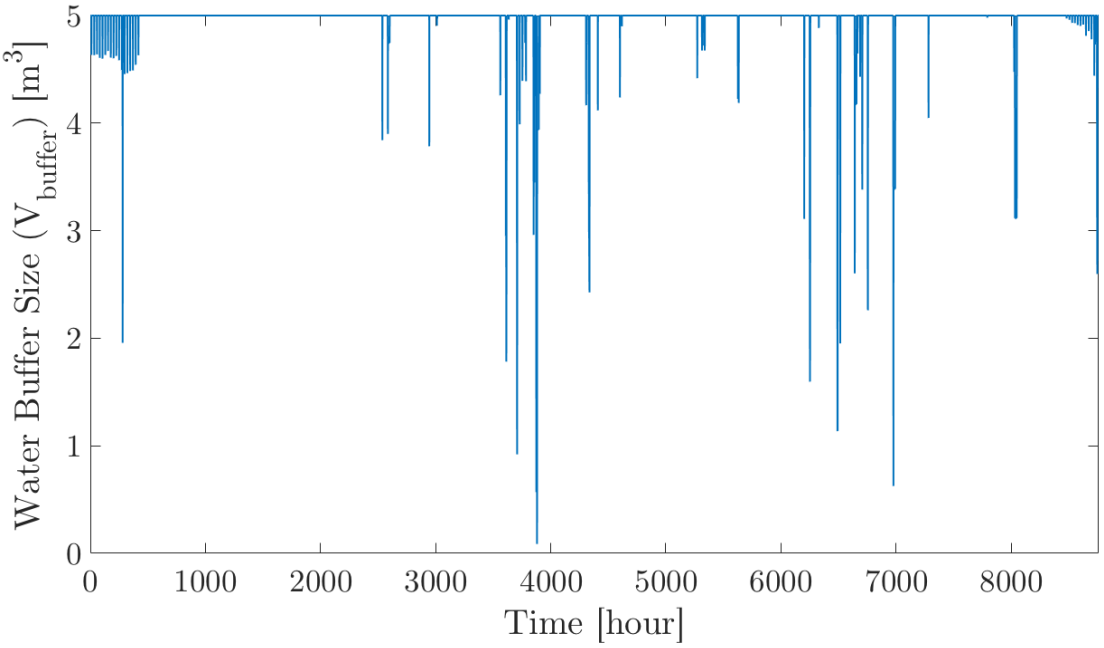

Figure 6-3: Buffer size as a function of time for the design solution of tomatoes (run 1).

Populations and Stopping Criteria

As shown in Figure 6-4, the GA stopped due to the stall generation, meaning that the algorithm could not produce a better solution for 500 generations. Technically, the first "best" solution was found within 100 generations .

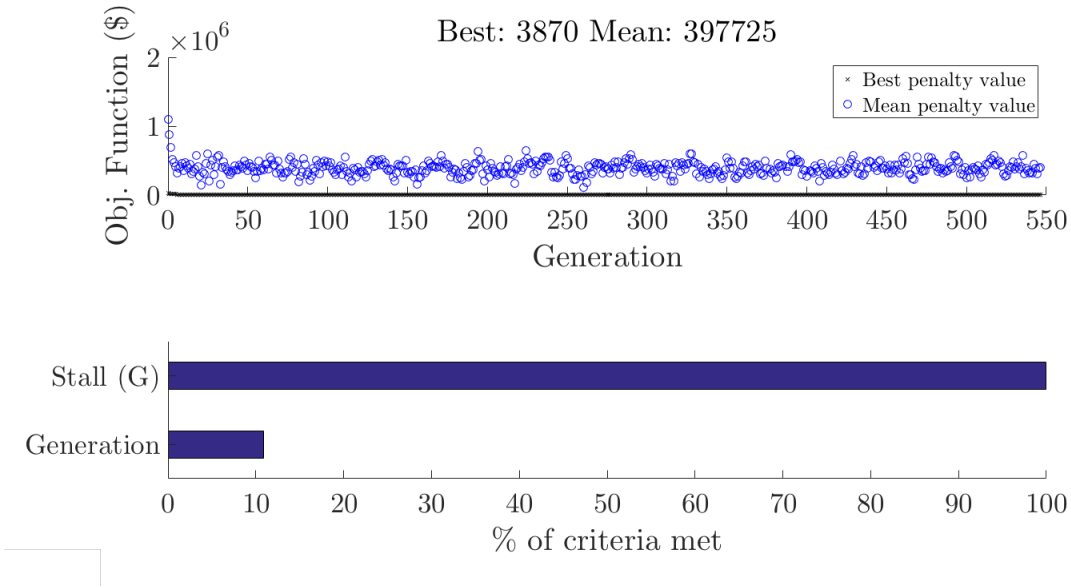

Figure 6-4: Best objective function per population and stopping criteria for tomatoes (Run 2). Each generation plots a mean objective value (blue circles) and best objective value (black x marks).

6.2.3 Crop: Barley

	Run 1	**Run 2**	**Run 3**
N_{solar}	3	3	3
V_{buffer} (m^3)	4	4	4
α $(^\circ)$	10	17	30
β $(^\circ)$	303	297	321
i_{panel}	SNMM320724BB	AE305M672	AE305M672
i_{pump}	PS600 CS-F4-3	PS600 CS-F4-3	PS600 CS-F4-3
t_{start}	9	9	8
t_{end}	16	16	16
Cost ($)	3,750	3,750	3,750
Runtime (sec)	4,566	4,499	5,947

Table 6.4: Results of GA for barley.

As shown in Table 6.4, the objective function of Run 1, Run 2, and Run 3 converged to $3,750. Although these runs had the same N_{solar} and V_{buffer}, their α and β are slightly different. As mentioned before this is due to the fact that the water output fairly insensitive to α and β. For barley, like the previous two crops, it is also shown that α can vary by several degrees and that β can vary by tens of degrees while

maintaining within all objective constraints.

Water Buffer (V_{buffer}) Analysis

The major objective constraint is to keep $V_{buffer} \geq 0$ for the entire year. In order to do a sensitive analysis, the buffer size as a function of time was analyzed.

As shown in Figure 6-5, the buffer is not utilized until the end of the year. This design solution easily stays above 0, fulfilling the objective constraint.

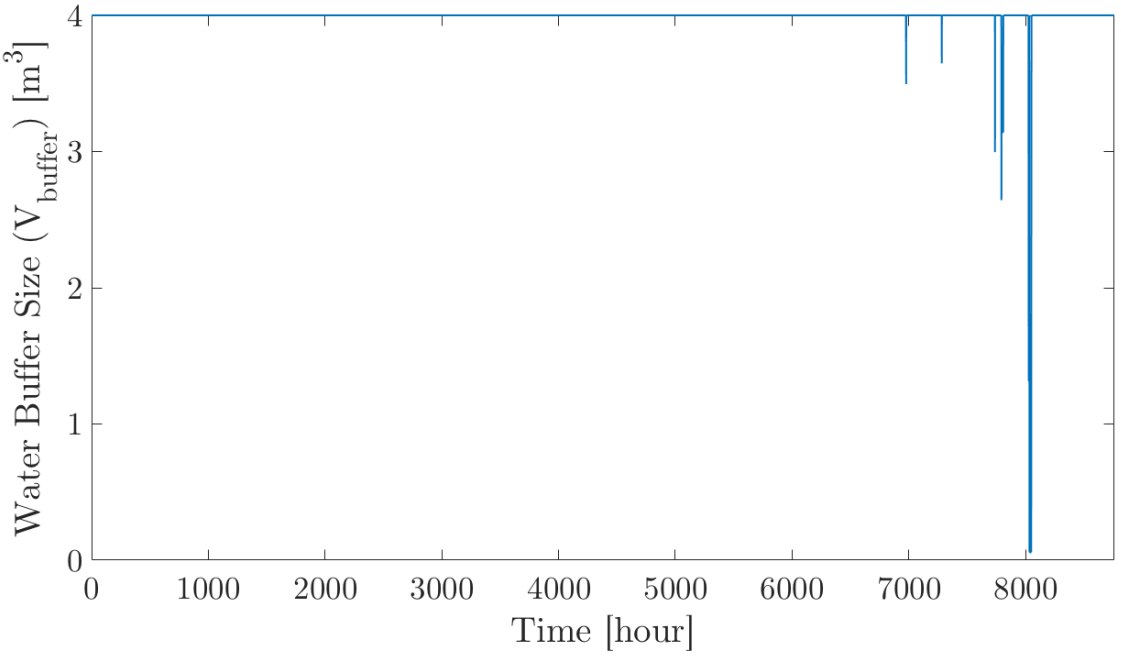

Figure 6-5: Buffer size as a function of time for the design solution of barley (run 1).

Populations and Stopping Criteria

As shown in Figure 6-6, the GA stopped due to the stall generation, meaning that the algorithm could not produce a better solution for 500 generations. In this case, the total number of generations is higher that those of the last two crops because the algorithm found a new minimum after a certain time, causing the stall generation criteria to reset.

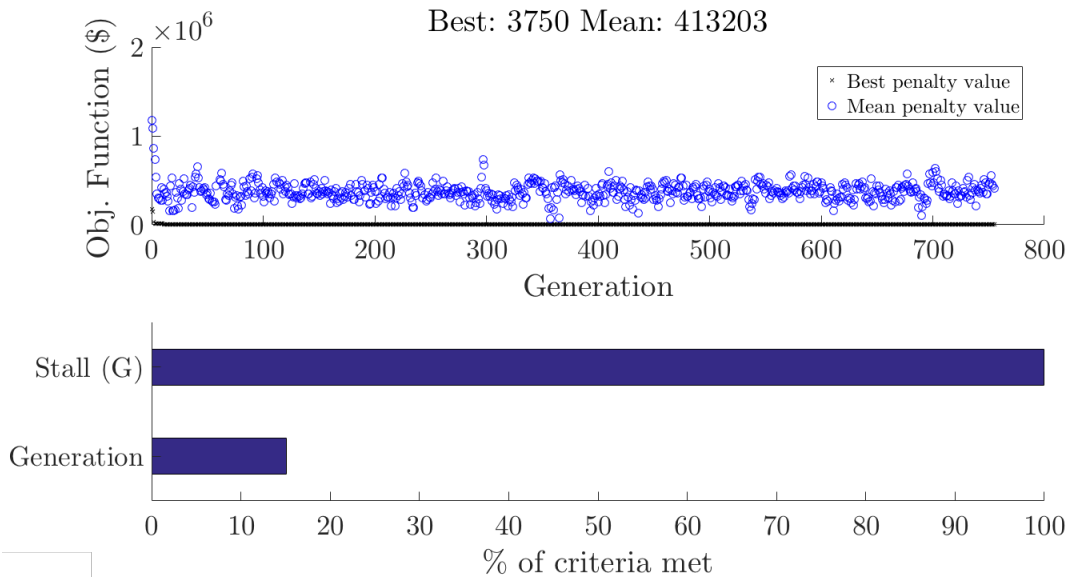

Figure 6-6: Best objective function per population and stopping criteria for barley (Run 1). Each generation plots a mean objective value (blue circles) and best objective value (black x marks).

Chapter 7

Conclusions and Future Work

This study shows the motivation, methodology, design, and results of a cost optimization for low-cost, solar-powered drip-irrigation systems. This framework will help in the decision making and design of solar-powered, drip-irrigation systems.

7.1 Future Work

Although the design is fairly comprehensive in its analysis on a systems level, there is still substantial work needed to ensure the accuracy and validity of this methodology. This includes implementing statistical analysis and probability, improving water pump and consumption analysis, improving cost analysis, implementing sensitivity analysis, improving optimization, and implementing experimental validation of each design module.

7.1.1 Statistical Analysis and Probability

As mentioned in Section 2.4.1, there is an outline for modelling the solar irradiance given historical data. This can be used to predict the amount of solar irradiance available for each given hour over the entire year. Given this, the model can then take another design variable, such as uptime, in order to give the farmer more fidelity when choosing a solar-powered, drip-irrigation system. For example, reducing the

uptime to 80%, rather than 100% (current design), may reduce the cost significantly and putting it within economic reach for the farmer.

7.1.2 Water Pump Analysis

The current method simply uses the manufacturer's pump curve and linear interpolation as a way to predict water output. However, the current model does not consider the coupling between the voltage of the solar panels and the pump itself. In addition, the model does not compensate for different pressure heads. In order to better understand the water pump's actual characteristics, this analysis must be done.

7.1.3 Water Consumption Analysis

Although the water consumption analysis is based on empirical data of the given crop, the environmental data of the specific location is not implemented. This includes variables such as temperature, humidity, and precipitation that would affect the water consumption of the crop, which may have a large effect on the amount of water needed in certain seasons.

7.1.4 Cost Analysis

The cost analysis of this model is lacking in compensating for installation costs, pump costs, and irrigation costs due to the large variability depending on location. In addition, large subsidies from the government may play a huge role in the economic viability of solar-powered, drip-irrigation systems.

7.1.5 Sensitivity Analysis

Although some sensitivity analysis is mentioned, a complete sensitivity analysis of each variable would be beneficial to the decision making and ability for variations in installation (for the case of tilt and azimuth angle).

7.1.6 Optimization

Although the results were successful in providing a feasile and relatively converging solution, there could be more improvements on the optimization parameters to increase run time and accuracy. For one, the stall and functional tolerances can be shown to be more lenient, as the minimum is reached within a fairly short number of generation. In addition, to prove convergence, or the decrease run time, an initial solution vector can be imposed.

7.1.7 Validation

Because of the scope of the thesis, validation was not completed for any of the modules. Validation of the solar modeling as well as water output modeling would be key in moving forward with confidence. This can be done by placing PV modules at a location in which solar data is available and comparing the actual power output to the predicted power output from the model. Going further, the PV system can be connected to a water pump to compare actual water output and to the estimated water output.

Overall, this thesis provides a starting framework for the cost optimization of solar-powered, drip-irrigation systems given historical data, location, and plant data.

Appendix A

SPA MATLAB Algorithm

```
% Solar Position Algorithm for Solar Radiation Applications
% Authors: Ibrahim Reda and Afshin Andreas
% Code By: David Doan | MIT 2017

function [azimuthAngle, zenithAngle, incidenceAngle, delta, ...
    hourAngle] = SPA(day, month, year, hour, minute, second, ...
    timezone, latitude, longitude, elevation, pressure, temperature, ...
    omega, gamma)
%% Polynomial Expression for Delta T
% (https://eclipse.gsfc.nasa.gov/SEcat5/deltatpoly.html)
deltaTPoly = [0.00002373599, 0.000651814, 0.0017275, -0.060374, ...
    0.3345, 63.86; 0, 0, 0, 0.005589, 0.32217, 62.92];
if year < 2005
    deltaTPoly = deltaTPoly(1,:);
else
    deltaTPoly = deltaTPoly(2,:);
end
deltaT = polyval(deltaTPoly,year-2000); % [seconds] deltaT in a ...
    given year
%% Julian Calendar Calculations
julianDay = juliandate(year, month, day, hour, minute, second);
julianDay = julianDay - (timezone/24);
```

```
18 julianDayEph = julianDay + deltaT/86400;
19 julianCentury = (julianDay - 2451545)/36525;
20 julianCenturyEph = (julianDayEph - 2451545)/36525;
21 julianEphMill = julianCenturyEph/10;
22 %% Heliocentric Constants and Calculations
23 L0 = [175347046 0  0; 3341656 4.6692568 6283.07585; 34894 4.6261 ...
       12566.1517; 3497 2.7441 5753.3849; 3418 2.8289 3.5231; 3136 ...
       3.6277 77713.7715; 2676 4.4181 7860.4194; 2343 6.1352 3930.2097; ...
       1324 0.7425 11506.7698; 1273 2.0371 529.691; 1199 1.1096 ...
       1577.3435; 990 5.233 5884.927; 902 2.045 26.298; 857 3.508 ...
       398.149; 780 1.179 5223.694; 753 2.533 5507.553; 505 4.583 ...
       18849.228; 492 4.205 775.523; 357 2.92 0.067; 317 5.849 ...
       11790.629; 284 1.899 796.298; 271 0.315 10977.079; 243 0.345 ...
       5486.778; 206 4.806 2544.314; 205 1.869 5573.143; 202 2.458 ...
       6069.777; 156 0.833 213.299; 132 3.411 2942.463; 126 1.083 ...
       20.775; 115 0.645 0.98; 103 0.636 4694.003; 102 0.976 15720.839; ...
       102 4.267 7.114; 99 6.21 2146.17; 98 0.68 155.42; 86 5.98 ...
       161000.69; 85 1.3 6275.96; 85 3.67 71430.7; 80 1.81 17260.15; 79 ...
       3.04 12036.46; 75 1.76 5088.63; 74 3.5 3154.69; 74 4.68 801.82; ...
       70 0.83 9437.76; 62 3.98 8827.39; 61 1.82 7084.9; 57 2.78 ...
       6286.6; 56 4.39 14143.5; 56 3.47 6279.55; 52 0.19 12139.55; 52 ...
       1.33 1748.02; 51 0.28 5856.48; 49 0.49 1194.45; 41 5.37 8429.24; ...
       41 2.4 19651.05; 39 6.17 10447.39; 37 6.04 10213.29; 37 2.57 ...
       1059.38; 36 1.71 2352.87; 36 1.78 6812.77; 33 0.59 17789.85; 30 ...
       0.44 83996.85; 30 2.74 1349.87; 25 3.16 4690.48];
24 L1 = [628331966747 0 0; 206059 2.678235 6283.07585; 4303 2.6351 ...
       12566.1517; 425 1.59 3.523; 119 5.796 26.298; 109 2.966 ...
       1577.344; 93 2.59 18849.23; 72 1.14 529.69; 68 1.87 398.15; 67 ...
       4.41 5507.55; 59 2.89 5223.69; 56 2.17 155.42; 45 0.4 796.3; 36 ...
       0.47 775.52; 29 2.65 7.11; 21 5.34 0.98; 19 1.85 5486.78; 19 ...
       4.97 213.3; 17 2.99 6275.96; 16 0.03 2544.31; 16 1.43 2146.17; ...
       15 1.21 10977.08; 12 2.83 1748.02; 12 3.26 5088.63; 12 5.27 ...
       1194.45; 12 2.08 4694; 11 0.77 553.57; 10 1.3 6286.6; 10 4.24 ...
       1349.87; 9 2.7 242.73; 9 5.64 951.72; 8 5.3 2352.87; 6 2.65 ...
       9437.76; 6 4.67 4690.48];
25 L2 = [52919 0 0; 8720 1.0721 6283.0758; 309 0.867 12566.152; 27 0.05 ...
```

```
    3.52; 16 5.19 26.3; 16 3.68 155.42; 10 0.76 18849.23; 9 2.06 ...
    77713.77; 7 0.83 775.52; 5 4.66 1577.34; 4 1.03 7.11; 4 3.44 ...
    5573.14; 3 5.14 796.3; 3 6.05 5507.55; 3 1.19 242.73; 3 6.12 ...
    529.69; 3 0.31 398.15; 3 2.28 553.57; 2 4.38 5223.69; 2 3.75 0.98];
L3 = [289 5.844 6283.076; 35 0 0; 17 5.49 12566.15; 3 5.2 155.42; 1 ...
    4.72 3.52; 1 5.3 18849.23; 1 5.97 242.73];
L4 = [114 3.142 0; 8 4.13 6283.08; 1 3.84 12566.15];
L5 = [1 3.14 0];
B0 = [280 3.199 84334.662; 102 5.422 5507.553; 80 3.88 5223.69; 44 ...
    3.7 2352.87; 32 4 1577.34];
B1 = [9 3.9 5507.55; 6 1.73 5223.69];
R0 = [100013989 0 0; 1670700 3.0984635 6283.07585; 13956 3.05525 ...
    12566.1517; 3084 5.1985 77713.7715; 1628 1.1739 5753.3849; 1576 ...
    2.8469 7860.4194; 925 5.453 11506.77; 542 4.564 3930.21; 472 ...
    3.661 5884.927; 346 0.964 5507.553; 329 5.9 5223.694; 307 0.299 ...
    5573.143; 243 4.273 11790.629; 212 5.847 1577.344; 186 5.022 ...
    10977.079; 175 3.012 18849.228; 110 5.055 5486.778; 98 0.89 ...
    6069.78; 86 5.69 15720.84; 86 1.27 161000.69; 65 0.27 17260.15; ...
    63 0.92 529.69; 57 2.01 83996.85; 56 5.24 71430.7; 49 3.25 ...
    2544.31; 47 2.58 775.52; 45 5.54 9437.76; 43 6.01 6275.96; 39 ...
    5.36 4694; 38 2.39 8827.39; 37 0.83 19651.05; 37 4.9 12139.55; ...
    36 1.67 12036.46; 35 1.84 2942.46; 33 0.24 7084.9; 32 0.18 ...
    5088.63; 32 1.78 398.15; 28 1.21 6286.6; 28 1.9 6279.55; 26 4.59 ...
    10447.39];
R1 = [103019 1.10749 6283.07585; 1721 1.0644 12566.1517; 702 3.142 ...
    0; 32 1.02 18849.23; 31 2.84 5507.55; 25 1.32 5223.69; 18 1.42 ...
    1577.34; 10 5.91 10977.08; 9 1.42 6275.96; 9 0.27 5486.78];
R2 = [4359 5.7846 6283.0758; 124 5.579 12566.152;  12 3.14 0; 9 3.63 ...
    77713.77; 6 1.87 5573.14; 3 5.47 18849.23];
R3 = [145 4.273 6283.076; 7 3.92 12566.15];
R4 = [4 2.56 6283.08];

sumL0 = SPA_heliocentric(L0, julianEphMill);
sumL1 = SPA_heliocentric(L1, julianEphMill);
sumL2 = SPA_heliocentric(L2, julianEphMill);
sumL3 = SPA_heliocentric(L3, julianEphMill);
```

```
41 sumL4 = SPA_heliocentric(L4, julianEphMill);
42 sumL5 = SPA_heliocentric(L5, julianEphMill);
43
44 L = (sumL0 + sumL1*julianEphMill + sumL2*julianEphMill^2 + ...
       sumL3*julianEphMill^3 + sumL4*julianEphMill^4 + ...
       sumL5*julianEphMill^5)/10^8;
45 L = radtodeg(L);
46 LMod = mod(L, 360);
47
48 if L > 0
49     L = LMod;
50 else
51     L = 360 - LMod;
52 end
53
54 sumB0 = SPA_heliocentric(B0, julianEphMill);
55 sumB1 = SPA_heliocentric(B1, julianEphMill);
56
57 B = (sumB0 + sumB1*julianEphMill)/10^8;
58 B = radtodeg(B);
59
60 sumR0 = SPA_heliocentric(R0, julianEphMill);
61 sumR1 = SPA_heliocentric(R1, julianEphMill);
62 sumR2 = SPA_heliocentric(R2, julianEphMill);
63 sumR3 = SPA_heliocentric(R3, julianEphMill);
64 sumR4 = SPA_heliocentric(R4, julianEphMill);
65
66 R = (sumR0 + sumR1*julianEphMill + sumR2*julianEphMill^2 + ...
       sumR3*julianEphMill^3 + sumR4*julianEphMill^4)/10^8;
67 %% Geocentric Longitude and Latitude Calculations
68 theta = L+180;
69 thetaMod = mod(theta,360);
70
71 if theta > 0
72     theta = thetaMod;
73 else
```

```
74      theta = 360 - thetaMod;
75  end
76
77  Beta = -B;
78  %% Longitude and Obliquity Calculations
79  X(1) = 297.85036 + 445267.111480*julianCenturyEph  - ...
        0.0019142*julianCenturyEph ^2 + julianCenturyEph ^3/189474;
80  X(2) = 357.52772 + 35999.050340*julianCenturyEph  - ...
        0.0001603*julianCenturyEph ^2 - julianCenturyEph ^3/300000;
81  X(3) = 134.96298 + 477198.867398*julianCenturyEph  + ...
        0.0086972*julianCenturyEph ^2 + julianCenturyEph ^3/56250;
82  X(4) = 93.27191 + 483202.017538*julianCenturyEph  - ...
        0.0036825*julianCenturyEph ^2 + julianCenturyEph ^3/327270;
83  X(5) = 125.04452 - 1934.136261*julianCenturyEph  + ...
        0.0020708*julianCenturyEph  ^2 + julianCenturyEph  ^3/450000;
84
85  Y  = [0 0 0 0 1 -171996 -174.2 92025 8.9; -2 0 0 2 2 -13187 -1.6 ...
        5736 -3.1; 0 0 0 2 2 -2274 -0.2 977 -0.5; 0 0 0 0 2 2062 0.2 ...
        -895 0.5; 0 1 0 0 0 1426 -3.4 54 -0.1; 0 0 1 0 0 712 0.1 -7 0; ...
        -2 1 0 2 2 -517 1.2 224 -0.6; 0 0 0 2 1 -386 -0.4 200 0; 0 0 1 2 ...
        2 -301 0 129 -0.1; -2 -1 0 2 2 217 -0.5 -95 0.3; -2 0 1 0 0 -158 ...
        0 0 0; -2 0 0 2 1 129 0.1 -70 0; 0 0 -1 2 2 123 0 -53 0; 2 0 0 0 ...
        0 63 0 0 0; 0 0 1 0 1 63 0.1 -33 0; 2 0 -1 2 2 -59 0 26 0; 0 0 ...
        -1 0 1 -58 -0.1 32 0; 0 0 1 2 1 -51 0 27 0;  -2 0 2 0 0 48 0 0 ...
        0; 0 0 -2 2 1 46 0 -24 0; 2 0 0 2 2 -38 0 16 0; 0 0 2 2 2 -31 0 ...
        13 0; 0 0 2 0 0 29 0 0 0; -2 0 1 2 2 29 0 -12 0; 0 0 0 2 0 26 0 ...
        0 0; -2 0 0 2 0 -22 0 0 0; 0 0 -1 2 1 21 0 -10 0; 0 2 0 0 0 17 ...
        -0.1 0 0; 2 0 -1 0 1 16 0 -8 0; -2 2 0 2 2 -16 0.1 7 0; 0 1 0 0 ...
        1 -15 0 9 0; -2 0 1 0 1 -13 0 7 0; 0 -1 0 0 1 -12 0 6 0; 0 0 2 ...
        -2 0 11 0 0 0; 2 0 -1 2 1 -10 0 5 0; 2 0 1 2 2 -8  0 3 0; 0 1 0 ...
        2 2 7 0 -3 0; -2 1 1 0 0 -7 0 0 0; 0 -1 0 2 2 -7 0 3 0; 2 0 0 2 ...
        1 -7 0 3 0; 2 0 1 0 0 6 0 0 0; -2 0 2 2 2 6 0 -3 0; -2 0 1 2 1 6 ...
        0 -3 0; 2 0 -2 0 1 -6 0 3 0; 2 0 0 0 1 -6 0 3 0; 0 -1 1 0 0 5 0 ...
        0 0; -2 -1 0 2 1 -5 0 3 0; -2 0 0 0 1 -5 0 3 0; 0 0 2 2 1 -5 0 3 ...
        0; -2 0 2 0 1 4 0 0 0; -2 1 0 2 1 4 0 0 0; 0 0 1 -2 0 4 0 0 0; ...
        -1 0 1 0 0 -4 0 0 0; -2 1 0 0 0 -4 0 0 0; 1 0 0 0 0 -4 0 0 0; 0 ...
```

```
    0 1 2 0 3 0 0 0; 0 0 -2 2 2 -3 0 0 0; -1 -1 1 0 0 -3 0 0 0; 0 1 ...
    1 0 0 -3 0 0 0; 0 -1 1 2 2 -3 0 0 0; 2 -1 -1 2 2 -3 0 0 0; 0 0 3 ...
    2 2 -3 0 0 0; 2 -1 0 2 2 -3 0 0 0;];

for j  = 1:length(Y)
    for i  = 1:length(X)
        C(j,i) = X(i)*Y(j,i);
    end
    phi(j) = (Y(j,6) + (Y(j,7)*julianCenturyEph))*sind(sum(C(j,:)));
end

for k  = 1:length(Y)
    epsilon(k) = (Y(k,8) + (Y(k,9)*julianCenturyEph ...
       ))*cosd(sum(C(k,:)));
end

deltaPhi = sum(phi)/36000000;
deltaEpsilon = sum(epsilon)/36000000;
%% True Obliquity of the Ecliptic Calculation
U = julianEphMill/10;

epsilon0 = 84381.448 - 4680.93*U - 1.55*U^2 + 1999.25*U^3 - ...
    51.38*U^4 - 249.67*U^5 - 39.05*U^6 + 7.12*U^7 + 27.87*U^8 + ...
    5.79*U^9 + 2.45*U^10;
epsilon = (epsilon0/3600) + deltaEpsilon;

deltaTau = -20.4898/(3600*R);

lambda = theta+deltaPhi+deltaTau;

vu0 = 280.46061837 + 360.98564736629*(julianDay-2451545) + ...
    0.000387933*julianCentury^2 - (julianCentury^3)/38710000;
vu0Mod = mod(vu0, 360);

if vu0 > 0
    vu0 = vu0Mod;
```

```
115 else
116     vu0 = 360 - vu0Mod;
117 end
118 vu = vu0 + deltaPhi*cosd(epsilon);
119 %% Geocentric Sun Right Ascension Calcuation
120 alpha = atan2d((sind(lambda)*cosd(epsilon) - ...
       tand(Beta)*sind(epsilon)), cosd(lambda));
121 alpha = mod(alpha,360);
122 %% Geocentric Sun Declination
123 delta = asind(sind(Beta)*cosd(epsilon) + ...
       cosd(Beta)*sind(epsilon)*sind(lambda));
124 %% Local Hour Angle Observation
125 hourAngle = vu + longitude - alpha;
126 hourAngle = mod(hourAngle,360);
127
128 xi = 8.794/(3600*R);
129 u = atan(0.99664719 * tand(latitude));
130 x = cos(u) + elevation/6378140*cosd(latitude);
131 y = 0.99664719*sin(u) + (elevation/6378140)*sind(latitude);
132
133 deltaAlpha = atan2d((-x*sind(xi)*sind(hourAngle)), ...
       (cosd(delta)-(x*sind(xi)*cosd(hourAngle))));
134 alphaPrime = alpha + deltaAlpha;
135 deltaPrime = atan2d((sind(delta) - y*sind(xi))*cosd(deltaAlpha), ...
       (cosd(delta) - x*sind(xi)*cosd(hourAngle)));
136 %%  Topocentric Hour Angle Calculation
137 hourAnglePrime = hourAngle - deltaAlpha;
138 %% Topocentric Zenith Angle Calculation
139 e0 = asind(sind(latitude)*sind(deltaPrime) + ...
       cosd(latitude)*cosd(deltaPrime)*cosd(hourAnglePrime));
140 deltae = (pressure/1010)*(283/(273+temperature))*1.02/(60*tand(e0+ ...
       (10.3/(e0 +5.11))));
141 e = e0 + deltae;
142
143 zenithAngle = 90-e;
144 %% Topocentric Azimuth Angle Calculation
```

```
145 astroazimuthAngle = atan2d(sind(hourAnglePrime), ...
        (cosd(hourAnglePrime)*sind(latitude) - ...
        tand(deltaPrime)*cosd(latitude)));
146 astroazimuthAngle = mod(astroazimuthAngle, 360);
147
148 azimuthAngle = astroazimuthAngle + 180;
149 azimuthAngle = mod(azimuthAngle, 360);
150 %% Incidence Angle for Any Surface Orientation Calculation
151 incidenceAngle = acosd(cosd(zenithAngle)*cosd(omega) + ...
        (sind(omega)*sind(zenithAngle)*cosd((astroazimuthAngle)-gamma)));
152 incidenceAngle = incidenceAngle;
```

A.0.1 Heliocentric Function

```
1  % Heliocentric Function for SPA
2  % Authors: Ibrahim Reda and Afshin Andreas
3  % Code By: David Doan | MIT 2017
4
5  function value = SPA_heliocentric(array, julianEphMill)
6      [a,b] = size(array);
7      sumArray = zeros(b,1);
8      for i = 1:a
9          A = array(i,1);
10         B = array(i,2);
11         C = array(i,3);
12         sumArray(i) = A*cos(B+(C*julianEphMill));
13     end
14     value = sum(sumArray);
15 end
```

Bibliography

[1] G Fischer and G. K. Heilig. Population momentum and the demand on land and water resources. *Philosophical Transactions of the Royal Society B: Biological Sciences*, 352:869–889, 1997.

[2] Francis Richard Stephenson and Michael A Houlden. *Atlas of Historical Eclipse Maps: East Asia 1500 BC-AD 1900*. Cambridge University Press, 1986.

[3] A Henderson-Sellers and MF Wilson. Surface albedo data for climatic modeling. *Reviews of Geophysics*, 21(8):1743–1778, 1983.

[4] John Cleland. World Population Growth; Past, Present and Future. *Environmental and Resource Economics*, 55(4):543–554, 2013.

[5] Foley J Mueller N, Gerber J, Johnston M, Ray D, Ramankutty N. Closing yield gaps through nutrient and water management, 1991.

[6] Frank R Rijsberman. Water Scarcity : Fact or Fiction ? pages 1–14, 2004.

[7] Saskia Van der Kooij, Margreet Zwarteveen, Harm Boesveld, and Marcel Kuper. The efficiency of drip irrigation unpacked. *Agricultural Water Management*, 123:103–110, 2013.

[8] Joseph Alcamo, Thomas Henrichs, and Thomas Rösch. World Water in 2025 - Global modeling and scenario analysis for the World Commission on Water for the 21st Century. *Kassel World Water Series 2*, (2):47, 2000.

[9] Pulkit Shamshery et al. Modeling and designing the future of drip irrigation: a validated parametric analysis used to design low power, pressure compensating drip emitters. Master's thesis, Massachusetts Institute of Technology, 2016.

[10] A. Narayanamoorthy. Drip irrigation in India: Can it solve water scarcity? *Water Policy*, 6(2):117–130, 2004.

[11] Richard M. Swanson. A vision for crystalline silicon photovoltaics, aug 2006.

[12] Pulkit Shamshery. Topology Optimization of Online Pressure Compensating Drip Emitters to achieve Lower Activation Pressure.

[13] Akram Abdulameer Abood, M M Shourov Akter, Asaduzzaman Shoeb, Marko Gulin, Mario Vašak, Mato Baotic, and Christian A. Gueymard. Estimation of the global solar irradiance on tilted surfaces. *San Diego Solar Conference*, 6(2):462–469, 2015.

[14] M M Shourov Akter and Asaduzzaman Shoeb. A Novel Model to Calculate Global Tilted Irradiation (GTI) from Solar Variables Using Netcdf and Rstudio. 6(2):462–469, 2015.

[15] Ibrahim Reda and Afshin Andreas Nrel. Solar Position Algorithm for Solar Radiation Applications (Revised). *Nrel/Tp-560-34302*, (January):1–56, 2008.

[16] Leslie V Morrison and F Richard Stephenson. Historical values of the earth's clock error δ and the calculation of eclipses. *Journal for the History of Astronomy*, 35(3):327–336, 2004.

[17] Marko Gulin, Mario Vašak, and Mato Baotic. Estimation of the global solar irradiance on tilted surfaces. *17th International Conference on Electrical Drives and Power Electronics (EDPE 2013)*, (i):334–339, 2013.

[18] K. N. Shukla, Saroj Rangnekar, and K. Sudhakar. Comparative study of isotropic and anisotropic sky models to estimate solar radiation incident on tilted surface: A case study for Bhopal, India. *Energy Reports*, 1:96–103, 2015.

[19] G R Mather. ASHRAE 93-77 Instantaneous and All-Day Tests of the Sunpak Evacuated-Iube Collector. 102(November 1980), 2017.

[20] G Dawson. Incident Angle Modifiers for Flat- Plate Solar Collectors : Analysis of Measurement and Calculation Procedures. 104(November):349–357, 1982.

[21] J. H. Fatehi and K. J. Sauer. Modeling the incidence angle dependence of photovoltaic modules in pvsyst. In *2014 IEEE 40th Photovoltaic Specialist Conference (PVSC)*, pages 1335–1338, June 2014.

[22] A Mermoud. Pvsyst help section: Array thermal losses. *PVsyst SA, Satigny, Switzerland*, 2015.

[23] S. Armstrong and W. G. Hurley. A thermal model for photovoltaic panels under varying atmospheric conditions. *Applied Thermal Engineering*, 30(11-12):1488–1495, 2010.

[24] Swapnil Dubey, Jatin Narotam Sarvaiya, and Bharath Seshadri. Temperature dependent photovoltaic (PV) efficiency and its effect on PV production in the world - A review. *Energy Procedia*, 33:311–321, 2013.

[25] Mohammad Reza Maghami, Hashim Hizam, Chandima Gomes, Mohd Amran Radzi, Mohammad Ismael Rezadad, and Shahrooz Hajighorbani. Power loss due to soiling on solar panel: A review. *Renewable and Sustainable Energy Reviews*, 59:1307–1316, 2016.

[26] C Brouwer and M Heibloem. Irrigation water management: irrigation water needs. *Training manual*, 3, 1986.